U. PORTO

FEUP FACULDADE DE ENGENHARIA
UNIVERSIDADE DO PORTO

Energy management and storage to decarbonize high-performance computing centers

Liliana Silva Torres Rodrigues

Mestrado em Engenharia Eletrotécnica e de Computadores

Supervisor: Dr. Ricardo Bessa

October 25, 2023

Abstract

High-performance computing infrastructures' increasing use and significance has made their carbon emissions and costs a problem for a society concerned with both the digital and energy transitions. The state of the art and initiatives of today do not take a comprehensive approach to HPC systems (energy sources and carbon footprint, predictive management and optimization, novel cooling technologies, etc.).

Therefore, to decarbonize the functioning of these systems, energy efficiency and energy management methods are required, along with effective computing management. By creating frameworks that classify the many regions of data and computing centers where energy saving methods may be performed, energy efficiency can be addressed. The main goal is to assess the decarbonization potential of a supercomputer's energy management system utilizing multitemporal asset management while taking into account various carbon intensity scenarios for the country's power grid. In order to size the solution, it also includes the analysis and potential use of models for electrical energy storage systems.

This dissertation was developed within the scope of INESC TEC's "Sustainable HPC" project, which focuses on the development of an energy management solution that promotes the decarbonization of system operation, including energy efficiency procedures. This solution will enable greener operating procedures for future advanced computing facilities and data centers. The Deucalion supercomputer, to be installed at the Minho Advanced Computing Center, will serve as a "living laboratory" to test different energy conversion and storage technologies, as well as new developments in the energy management system. It is a supercomputer whose main feature is its processing: 10 Petaflops, i.e. 10 million billion calculations per second. Deucalion will offer services both for traditional HPC computing, AI and Big Data/HPDA analytics.

Keywords : Sustainable high-performance computing, Second life batteries, Vanadium redox-flow batteries, Energy management system

ii

Resumo

A utilização e a importância crescentes das infra-estruturas de computação de elevado desempenho tornaram as suas emissões de carbono e os seus custos um problema, para uma sociedade preocupada com as transições digital e energética. O estado da arte neste momento, bem como as iniciativas atuais, não adotam uma abordagem abrangente dos sistemas HPC (fontes de energia e pegada de carbono, gestão e otimização preditivas, novas tecnologias de arrefecimento, etc.).

Por conseguinte, para descarbonizar o funcionamento destes sistemas, são necessários métodos de eficiência energética e de gestão da energia, juntamente com uma gestão eficaz da computação. Ao criar quadros que classificam as muitas regiões dos centros de dados e de computação onde podem ser aplicados métodos de poupança de energia, a eficiência energética pode ser abordada. O principal objetivo é avaliar o potencial de descarbonização do sistema de gestão de energia de um supercomputador, utilizando a gestão multitemporal de ativos, e tendo em conta vários cenários de intensidade de carbono para a rede eléctrica do país. A análise e potencial utilização de modelos para sistemas de armazenamento de energia eléctrica são também incluídas nas formas de dimensionamento da solução.

Esta dissertação foi desenvolvida no âmbito do projeto "Sustainbale HPC" do INESC TEC, que tem como foco o desenvolvimento de uma solução de gestão de energia que promova a descarbonização da operação do sistema, incluindo procedimentos de eficiência energética. Esta solução vai permitir procedimentos de operação mais ecológicos para futuras instalações de computação avançada e centros de dados. O supercomputador Deucalion, a instalar no Centro de Computação Avançada do Minho, servirá de "laboratório vivo" para testar diferentes tecnologias de conversão e armazenamento de energia, bem como novos desenvolvimentos no sistema de gestão de energia. Trata-se de um supercomputador cuja principal caraterística é o seu processamento: 10 Petaflops, ou seja, 10 milhões de biliões de cálculos por segundo. O Deucalion oferecerá serviços de computação HPC tradicional, de IA e de análise de Big Data/HPDA.

Palavras-Chave : Computação de elevado-desempenho sustentável, Baterias de segunda vida, Baterias de fluxo regenerativo de vanâdio, Sistema de gestão de energia

Agradecimentos

Aos meus pais, as pessoas mais importantes da minha vida, que desde me ensinaram a sonhar e a correr atrás desses sonhos de forma a torná-los realidade. Por todos os valores que me incutiram, por terem acreditado sempre em mim e nas minhas capacidades, às vezes até mais que eu própria, e por nunca me terem deixado desistir. Um obrigada não é suficiente para vocês.

Quero também agradecer às duas pessoas que me acompanharam no desenvolvimento desta dissertação, ao Dr. Ricardo Bessa, e em especial ao Carlos Silva por todo o conhecimento transmitido, o apoio e a orientação dada durante todo este tempo.

Ao Renato, um especial obrigada pela paciência. Sem dúvida, foste um suporte muito importante nas horas mais complicadas, e a primeira pessoa com quem eu contava, e continuo a contar, para festejar nos momentos mais felizes. Obrigada por todos os chocolates de motivação e pelos dotes culinários.

Aos 8 amiguinhos que me acompanham há 5 anos, os que viveram comigo o melhor da vida académica. Desde as explicações aos momentos de loucura, aos dias por aí num certo Jardim da FEUP, ou na I101. É bom ver-nos a acabar mais uma etapa juntos, como deve de ser.

Aos outros amigos todos também, em especial à Ana, a minha melhor amiga, que, no quarto ao lado ou do outro lado do mundo, é um apoio incondicional há muitos muitos anos .

E por último, mas não menos importante, a mim.

Liliana

To those who inspired it ,
and will not read it

Contents

List of Figures

List of Tables

Abbreviations and symbols

HPC   High Performance Computing
ENIAC   Electronic Numerical Integrator and Computer
GHG   Green House Gas
KPI   Key Performance Indicator
PUE   Power Use Effectiveness
CUE   Carbon Use Effectiveness
WUE   Water Use Effectiveness
EUE   Electronics Use Effectiveness
SOC   State of Charge
SOH   State of Health
ECM   Electric Circuit Model
RFB   Redox-Flow Batteries
IEM   Ion Exchange Membrane
VRFB   Vanadium Redox-Flow Batteries
EV   Electric Vehicles
PSO   Particle Swarm Optimization
EPSO   Evolutionary Particle Swarm Optimization
LCOE   Levalized Cost of Electricity
LCOS   Levalized Cost of Storage
NPV   Net Present Value

Chapter 1

Introduction

1.1 Motivation

It is now widely acknowledged that moving toward a sustainable future is important. To minimize negative environmental effects and cut greenhouse gas emissions throughout this transition, it is crucial to use energy resources efficiently and to use renewable energy sources. This topic is causing some concern, and awareness of it is growing. In 2015, the European Union's "Sustainable Development Goals" program included, among other objectives, the reduction of greenhouse gas emissions by at least 55%, and a significant increase in renewable energies, by 2030.

In this context, this dissertation aims to investigate how energy management and storage in high-performance computing centers can significantly contribute to that said sustainable transition. With the growing importance and use of these infrastructures, it becomes essential to understand how to optimize their energy efficiency and reduce their carbon footprint.

In addition, is also assessed the potential for adopting renewable energy sources to power these. The integration of clean energies can significantly reduce greenhouse gas emissions and contribute to a more ecoefficient computing system.

1.2 Problem Statement and methodologies

In order to address the problem present above, this work was divided into four main parts.

Initially, a detailed study was carried out, through literature review, in order to acquire knowledge about the current state of the art regarding each battery, as well as the issue of green computing and how it is approached in a real context.

Next, started the modelling of the optimization problem itself and all that it involves: the creation of the objective functions, constraints associated with them and identification of relevant information. This step was essential because it allowed to choose the algorithm to be used later when implementing the problem in Python.

1

In addition, a financial analysis of the problem was carried out, at an energy level, in which the price of storing 1 MW of energy in different devices was estimated, as well as the payback period for each technology used.

Finally, the results of this study were presented and analyzed in detail, along with possible future work and improvements to this study.

1.3   Dissertation's structure

This dissertation is divided into five chapters. In chapter 1, is presented an introduction that contextualizes the research problem and describes the objectives of the study. In addition, the main concepts and theoretical foundations that underpin the entire investigation are presented. In chapter 2, a literature review is carried out, whose main objective is to consolidate existing knowledge and identify gaps that will be addressed during the research. In chapter 3, the methodology adopted for this work is described along with all the procedures carried out. The case study is then described in detail in chapter 4, and the results obtained are presented (in the form of graphics and tables) and discussed. This chapter also includes the financial analysis of the project, as mentioned above. Finally, in chapter 5, the overall conclusions of the dissertation are presented and the main results are summarized. In addition, possible research directions for future work are also presented.

Chapter 2

State of the Art

High Performance Computing (HPC), also referred to as Supercomputing is an aggregation of computer power to solve problems that are either too large for standard computers or would take too long. It enables the simulation or analysis of huge volumes of data that would otherwise not be possible to process with those standard computers.

Since it produces or processes more data than the infrastructure resources can handle, the main problem focuses on the fact that it is necessary to wait weeks or even months to see the results, which delays the innovation and slows down research.

A HPC system can be seen as a group of computers - a cluster - in which each computer is called a node. Each node contains an operating system, a processor with multiple cores, storage, and network capabilities for the units to talk to each other.

A data center is a centralized repository containing a large number of processing nodes clustered together in order to store vast amounts of data [1]. Data centers host a lot of infrastructures, being supercomputers just one example of them.

Data centers date back to the 1940s, when the Electronic Numerical Integrator and Computer (ENIAC), the world's first programmable computer - used for military purposes during World War II - was the pinnacle of computational technology [2]. The first data centers to appear supported simple distributed applications running in them and were primarily used to serve data to customers outside the data center. With the evolution of technology and the demand for processing large amounts of data, some aspects of conventional high-performance computing were swiftly incorporated into data center network requirements [3].

2.1 Green Supercomputing

For decades, supercomputing has focused primarily on performance and, occasionally, on price/ performance ratio, which comes from the need to solve complex problems in different areas. However, focusing only on this parameter has caused other equally relevant parameters to be forgotten.

It is well known that maintaining large-scale supercomputers implies a huge consumption of energy, both in terms of powering them and ensuring that they are properly cooled - therefore, the

result is high operating costs [4]. That said, the main challenge associated with the level of consumption of the network is that there is, as mentioned above, a large demand for energy (necessary for the operation of supercomputers). The quality of this energy is also a very influential factor - supercomputers are sensitive to variations in power quality, which influences their performance and can even damage them. Energy costs and grid resiliency are other challenges to be met. Thus, collaboration between grid operators and supercomputing organizations is essential to ensure that energy demand is met.

Recently, there has been awareness of the environmental impact caused by HPC systems and the urgent need to reduce energy consumption and carbon footprint. Carbon footprint refers to the amount of Green House Gas (GHG) - which includes methane and mainly carbon dioxide - generated by the energy consumption of an individual or a system. There has also been awareness about the "carbon aware footprint". This is a comprehensive analysis that goes beyond the typical notion of "carbon footprint", as it incorporates all direct and indirect emissions over the full life cycle which, in the context of green supercomputing, is particularly relevant. The carbon footprint of a data center can be divided in three different classes: the one related to the manufacture and data center's purchased equipment, the one related from daily operations, and the one originated from en-of-life disposal of equipment of the data center [5].

GHG emissions from electricity production vary substantially due to various factors such as time and location. This variation in carbon intensity means that these factors have a significant effect on the associated global warming [6]. It is estimated that currently, computing and communication technology sectors are responsible for approximately 2% of global carbon emissions, with a tendency to annual increase of 6% [7].

Monitoring all data center components is necessary for its efficient and environmentally friendly operation. Energy efficiency in data centers refers the useful work done by various subsystems. It should be noted that it is possible to decrease carbon emissions in a data center by maintaining HPC operation: the solution passes by reducing electricity consumption through energy efficiency measures. This is especially relevant also in all the surrounding systems that make it operate safely, such as the cooling systems, where many energy efficiency measures have been implemented (water cooling instead of air cooling, for example). A panoply of key performance indicators (KPI) assists the measurement of different parameters in a data center (among them, energy efficiency).

Historically, HPC efficiency was measured by power efficiency (GFLOPS/W), however, due to the consumption of cooling systems, it is now measured in terms of Power Usage Effectiveness (PUE). This metric represents the ratio between the total system energy (electrical + cooling) and the electrical energy used by the IT equipment.

The PUE values can range from 1 to infinity, representing 1 a total of 100% efficiency by the equipment, i.e., all the energy would be used exclusively by the IT equipment (which obviously is not doable in real world due to the other support systems involved). Thus, the higher the PUE, the greater the amount of energy is being used for cooling or other non-computing purposes, which contributes to increase the carbon footprint. Sustainable data centers are very interested in increasing the energy efficiency of their powering and cooling systems, thus reducing PUE [8].

Recently, there has been a move to use new metrics, combined with the metrics once used. This new metrics are constantly being developed and used to meet evolving technologies and business needs. Green metrics measure the environmental impact of data center's components.

Carbon Usage Effectiveness (CUE), Water Usage Effectiveness (WUE) and Electronics Usage Effectiveness (EUE) have been proposed to measure carbon footprint, water consumption per year and disposal efficiency, and progressively adopted as the latest KPI in data centers [9].

Data center industry does, however, have the potential to reduce carbon emissions in the power grid: by properly managing its load, this industry can contribute to a more robust, resilient and cost-effective power system, ultimately facilitating grid decarbonization.

In recent years, there has been increasing talk around the concept of "green computing" [4]. Green computing, also known as sustainable computing, refers to the practice of maximizing energy efficiency while minimizing carbon emissions, thereby reducing the carbon footprint. Thus is the main point that distinguishes it from traditional computing. Done well, green computing reaps a number of environmental benefits.

2.2 Energy management in supercomputers/ data centers

The problem of pollution caused by high power consumption has already been addressed. It is known that continuous improvement in energy efficiency in existing data centers is an asset to reduce their environmental footprint [10]. But what strategies can be used to properly manage energy in these places?

Although there are some known successful techniques for reducing the energy consumed by hardware equipment (which includes IT, cooling and power supply systems), some researchers [8] believe that the only way to solve the problem is through a holistic approach, which involves adopting solutions that enable a synergistic and energy-aware management of data centers. It is understood that energy-aware management refers to the use of technologies and tactics to optimize energy use and raise energy efficiency within the infrastructure of data centers [11].

Some steps need to be taken in order to achieve the desired sustainability. First, it is essential to enable awareness of energy impact and carbon footprint (as discussed before).

Besides that, it is also important to increase the efficiency of hardware equipment which includes choosing processors, memory and storage devices that are designed to consume less power. Virtualizing a data center means that multiple servers, storage and network devices can be integrated into a virtualized one, in order to improve utilization of server resources [12].

Although there has been a noticeable evolution in hardware in data centers, especially in order to increase efficiency, it should be noted that this evolution has been incremental and slower. This is due to the focus on the infrastructure part of the data center itself. Investment in increasingly sustainable and efficient cooling solutions has grown exponentially. Among these stands out free cooling, which consists of using water or ambient air to cool the equipment.

Increasing the use of renewable energy sources is also an important step towards reducing data centers' carbon footprint. This practice introduces new challenges to data centers management.

One such challenge arises when using intermittent energy sources, i.e. sources that are not always available (like solar or wind energy) [8]. DER, which stands for Distributed Energy Resources, are small-scale power supply or demand resources that are connected to the electrical grid. On-site DER are power generating and energy storage systems that are installed and run right where energy is required [13] .

The choice of location for a data center is very important. For example, if a location with abundant wind energy sources is chosen, it will be easier to use wind energy to generate electricity; if the data center takes place in a cold region, the costs associated with it cooling system will be lower, etc. It is also essential to consider the cost of energy on the site (since this is a variable factor), which may or may not motivate the use of renewable energy. By examining the area's energy generating mix and the carbon intensity of the region, data centers are located in ways that attempt to have the least amount of of an environmental impact possible. The goal is to identify areas with a cleaner energy structure, where the majority of the electricity produced is from renewable resources.

In short, energy management is critical for supercomputers and data centers when it comes to reducing operating costs, maintaining good performance (or increase its quality) and reliability, and compliance with regulations.

2.2.1   Resource Sizing and optimal operation

Resource sizing, in a data center context, refers to the process of determining the optimal capacity of resources required to meet the computing and storage needs of it. It should be noted that "capacity resources" refers to capacity servers, storage devices and all other components needed to support operations in data center.

Data centers can use renewable energy resources, including solar power, to reduce the environmental impact. Solar PV (photovoltaic) systems are therefore considered a good option for implementation. It is necessary to take some factors into consideration when determining the storage capacity, as well as the PV installed capacity. This PV installed capacity will depend on the energy consumed by the infrastructure and the amount of energy that needs to be stored in the battery bank.

Basically, the sizing of the energy storage and PV system will depend on the specific needs of the supercomputer or data center.

After determining the resource requirements for an energy management system in a supercomputer or data center, the next step is to optimize the operation.

To formulate optimization problems, first, it is necessary to define the objective function (which will be the target problem of optimization), the decision variables (which are the control variables of the problem) and the applicable constraints. The type of signal used in these problems varies according to the objective of each and how it affects the operation of the data center.

In the specific case of data centers, optimization is an ongoing process and can occur at different intervals. The frequency of optimization is also dependent on various factors, among them the target components of the optimization, the goal of the optimization, etc.

2.3 Modelling of storage units

In order to implement energy management strategies through the formulation of an optimization problem, we need models that explain how to model battery storage systems, primarily related to their charging and discharging process, but also to their degradation over time.

Batteries have a relatively limited lifetime. Their performance is affected by some factors (internal or external), such as temperature, charge and discharge. It is, however, possible to predict how these factors will affect the lifetime of the battery and manage the number of cycles and therefore, part of the degradation and hence the life cycle.

There are a lot of key parameters to evaluate the performance of the battery, among them the state of charge (SOC), state of health (SOH), terminal voltage, discharge current, real capacity, impedance and losses.

It is essential to perform a proper study of the battery models since they have a fundamental character for determining the electrical and thermodynamic characteristics of the system and understanding the behavior of the battery itself under different conditions of use. They are, therefore essential tools for optimization problems, allowing the development of algorithms that consider the limitations and characteristics of the energy storage system, as well as the identification of optimal solutions for different objectives.

In [14] the authors discuss some of these, namely the bucket model, the equivalent circuit model and single particle model.

It is understood that "bucket model" refers to a simplified analogy used to represent the operation of the battery: it is seen as a bucket that stores electrical charge. When the bucket is full of water, it means that the battery is fully charged (maximum SOC), and the electrical charge is stored in the battery; when the battery is connected to a device it is as if the tap on the bucket is turned on - the water (electrical charge) starts to flow out of the bucket and into the device in question (leading to a decrease in the SOC of the battery). The voltage in the battery and the water level in the bucket relate in a directly proportional way. The main challenge associated with this model involves determining the size of the bucket as well as deciding when to fill or empty it in order to maximize the economic return of the project. This model will be presented and studied later in the section regarding the optimization of vanadium redox-flow batteries.

There are several types of battery modelling methods that can be used to simulate and predict their behavior. Figure 2.1 summarizes some, among which a few are mentioned again throughout this chapter.

Empirical models treat the voltage at the battery terminals as a function of SOC and current. They are considered a simplified version of the electrochemical models since they represent the nonlinear characteristics of the battery by using mathematical expressions and reducing their polynomial order.

Equivalent Circuit Models (ECM) are the most intuitive and easiest to analyze all the electrical components of the battery. Their component values are usually estimated using experimental
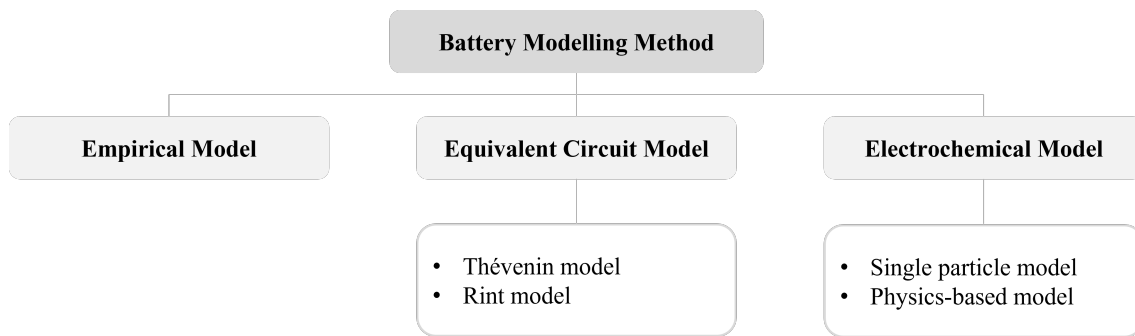
Figure 2.1: Classification of modelling methods

data. This category includes the Thévenin and Rint Equivalent Models (which will be particularly mentioned in the next subsections).

Finally, Electrochemical Models are intended to describe the reactions inside the battery. They involve solving complex sets of partial differential equations and often require a higher level of computational resources compared to other models.

Another approach to estimate the battery lifetime is through the use of different models that may or may not consider battery degradation over time.

2.3.1 Li-on batteries

Rechargeable batteries are a key-technology for developing many emerging applications, and have attracted a lot of attention. [15]

Lithium-ion batteries (often abbreviated as Li-ion batteries) are one of the most advanced rechargeable batteries and have impacted the microelectronics revolution, becoming the favorite power source for portable electronic devices (such as mobile phones and laptops), due to higher gravimeter and volumetric energy density they offer when compared to other rechargeable systems [16]. High energy density means storing a lot of energy in a small, lightweight pocket, which is due to the fact it operates at approximately 4V, a result of using water-free, non-aqueous electrolytes.

Besides these very small batteries, used essentially for electronics, there are Li-ion batteries of different sizes. Currently, they are popular as devices with great potential to be the major energy storage in off-grid renewable energy (although the field of energy storage industry is constantly developing, with new solutions appearing on a regular basis).

Their operating principle involves the transfer of lithium ions between a cathode (the positive electrode, usually made of a transition metal oxide) and an anode (the negative electrode, usually made of a carbon-based material) through an electrolyte (an ionic solution that allows the transfer of ions) during the charge and discharge processes.

The physical construction boils down to connecting basic Li-ion cells in parallel (if the objective is to increase the current) or in series (if the goal is to increase the voltage). [17]

Li-ion batteries and photovoltaic (PV) systems are often used together in order to increase the efficiency and reliability of renewable energy sources. PV systems convert solar energy into

electrical energy, while batteries store this same energy for later use. This combination can also be advantageous in reducing the cost of electricity: by storing excess energy during periods of low demand, and then using it during periods of high demand, it is possible to reduce the need for expensive power plants during peak load periods.

Nowadays, there is talk of another important expanding market - electric and hybrid vehicles - which requires next-generation Li-ion batteries, not only with high power but also with high capacity, charging rate, and long life.

2.3.1.1 Battery Model

There are a huge variety of mathematical and electric equivalent circuit models capable of describing the processes present in Li-ion batteries. The dynamic resistive-capacitor model, the active-resistive battery model, and the first and second Thévenin models occupy a prominent place. The model selected to be discussed in this subsection is the one prevenient from the original work of Chen and Ricón Mora [18]
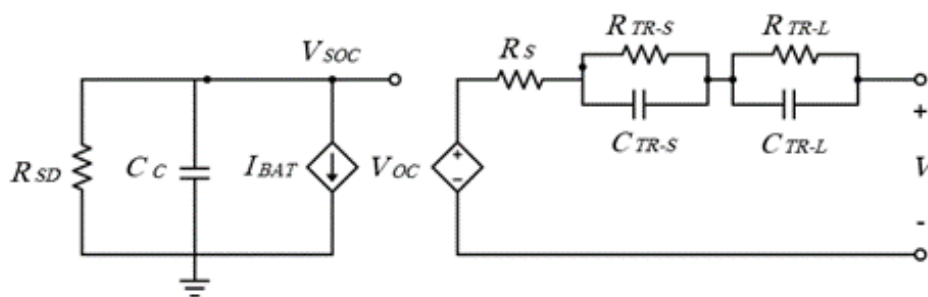
Figure 2.2: Chen and Ricón Mora equivalent circuit, adapted from [18]

It is a combined electrical model (composed of two circuits, connected by V_{SOC}) capable of predicting the battery run-time.

The circuit on the left is composed of a self-discharge resistance (R_{SD}), a capacitor (C_{CAP}) and a controlled current-source (I_{BAT}). The function of this part is to model the capacity, the SOC, and the battery life.

On the right, there's the Thévenin equivalent circuit. It is composed of two RC networks connected in parallel, a resistor (R_{SR}) and a controlled voltage source (V_{OC}). This part is responsible for modeling the transient response. The elements R_{TR-S}, C_{TR-S} and R_{TR-L} represent the short transient response. The element C_{TR-L} represents the long transient response.

It is possible to perform a more detailed analysis of the circuit by applying Kirshoff's laws.

Different approaches are used for modeling li-ion batteries. The most realistic models are the physical-chemical ones, which go through a consideration of the aging effects, but only on a small time scale since they're very complex to parameterize. Numerous aging elements must be taken into account for an aging prediction.

2.3.1.2   Degradation of Li-ion batteries

The lifetime of a battery refers to the period during which it can perform at a given level before it is replaced or retired. Battery aging is a process simultaneous to energy exchanges, and when it is stored. This means that even if the battery is not in use, its internal degradation is still happening. As such, this degradation is an unavoidable process that occurs either with time (calendar aging) or with use (cycle aging) and includes loss of capacity and internal resistance rise - the most relevant parameters to determine battery aging or SOH.

The term "cycling life" refers to the number of charge and discharge cycles that a battery can complete before it begins to lose performance [19]. Each of these cycles translates into an amount of irreversible capacity loss that accumulates over time, eventually leading to a reduction in battery capacity and therefore performance.

As mentioned earlier, the degradation of li-ion batteries is not just due to battery use. Calendar aging is a type of aging caused by the natural degradation of the battery's materials and components, as well as by the accumulation of impurities that reduce its performance.

There are several factors that contribute to the capacity fading of li-ion batteries, among them temperature, state of charge (SOC), current rate (C-rate), and depth of discharge.

Temperature is one of the most important factors affecting battery life (cycling and calendar speaking, making this a key factor to consider). There are several factors that influence the temperature, among them the ambient temperature (influenced by geographical location, climate, season, etc.), the self-heating process, heat capacity, thermal conductivity, and even the thermal management system itself [20]. Generally speaking, the effects of temperature are more visibly present in cell failure than in a reduction in cycle life.

The battery SOC has a major impact on battery life as well. There is a strong correlation between the SOC and the voltage in a battery, so these are shown to be dependent variables. However, this relationship is also affected by other factors (such as battery chemistry), so it is characterized by its non-linearity.

The battery voltage decreases as the SOC decreases, and if the SOC were too low, the disorder of the structure of the active material of the cathode and the corrosion of the copper current collector of the anode would significantly reduce battery life [21].

On the other hand, a high SOC means a high terminal voltage and, consequently, a lower anode potential and a higher cathode [20].

Because there are so many factors influencing the degradation of batteries, modeling their degradation is a multi-parameter and non-linear process [19]. There are two major approaches to modeling: empirical and physically based [22].

For the purpose of creating high-performance batteries that will satisfy the needs of various applications, understanding battery degradation is essential.

2.3.2 Second-life batteries

The conversation around battery reuse arose when the first commercial electric vehicles (EV) appeared and, since then, it has been a topic of much research and experiments [23].

Second-life batteries are batteries that have previously been used in other applications, however, they still have significant energy storage capacity, which allows them to still be used as stationary energy storage systems. Figure 2.3 illustrates this process.
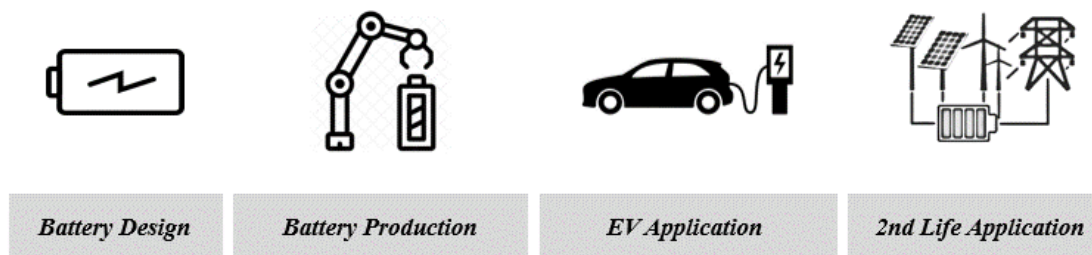
Figure 2.3: Life cycle of EV second-life batteries

This second-life phenomenon has positive aspects, such as lowering manufacturing costs and mitigating waste generated by direct disposal and, as expected, it also has a couple of challenges that include battery collection, storage and recycling [24].

The growing demand for Li-ion batteries has led to concerns regarding their incorrect disposal since their constituents are considered harmful to health and the environment. The materials used in these batteries are not cheap, so retiring them after only one use spells into economic waste [25].

Similar to what happens with first life batteries, second life batteries also undergo degradation over time. As expected, their degradation rate is higher than the degradation rate of first life batteries. Knowledge of battery performance and degradation after its retirement is critical for assessing the economic and environmental performance of second-life batteries [23].

The lifetime of a battery is expressed in a number of charge/discharge cycles and represents its expected longevity. Identifying the optimum point to retire a Li-ion battery is crucial in order to maximize the overall benefit across its first and second life [24].

A Li-ion cell has a typical lifespan of 500 to 3000 cycles. When a cell has reached 80% of its initial capacity, it is considered exhausted. It should be noted, however, that a disposed cell does not abruptly stop working (as mentioned above) – it can still work for about 2000 more cycles before its effective capacity falls to 60% and it shows significant voltage losses from the aging process [26].

2.3.2.1 Battery models

ECM is among the most used ways to model second-life battery applications.

Figure 2.4 represents an ECM that provides a true representation of the battery SOC, the number of cycles in the battery voltage, and the energy losses by self-discharge.
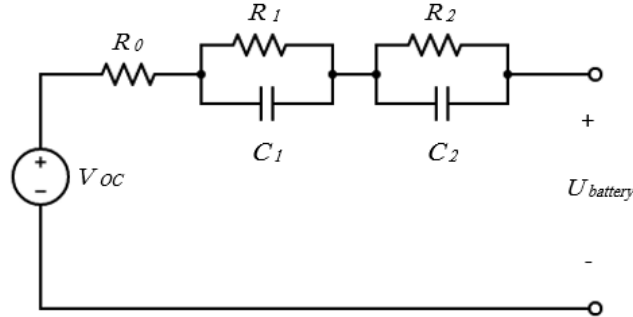
Figure 2.4: Schematic diagram of a battery cell ECM, adapted from [27]

The voltage variations are calculated using the following equation:

$$U_t = V_{OC} - IR_1 e^{-\frac{t}{\tau 1}} - IR_2 e^{-\frac{t}{\tau 2}} \tag{2.1}$$

where:

$$\tau 1 = R_1 C_1 \tag{2.2}$$

$$\tau 2 = R_2 C_2 \tag{2.3}$$

The model presented above allows for the prediction of parameter variations related to second life batteries [27]. This makes possible a more efficient management of the system, allowing a longer system lifespan.

2.3.3 Redox-flow batteries

Redox-flow batteries (RFB) belong to the category of electrochemical storage systems. The key component of RFB, when compared to other electrochemical storage systems, lies in the fact that it separates power and energy, allowing them to be tailored for specific applications.

Their development started in the 70s, to be part of the United States space program regarding energy storage for long-duration space missions. In the following decade, the possibility of using these batteries for energy storage in a grid context, i.e., storing energy produced by renewable sources and making it available when needed, was studied. Recently, the requirement for switching from fossil to renewable energy sources has accelerated the development of large-scale energy storage solutions.

The working principle behind these batteries is identical to any other ones: oxidation-reduction reactions. However, this reaction occurs between two electrolytes (an anolyte and a catholyte),
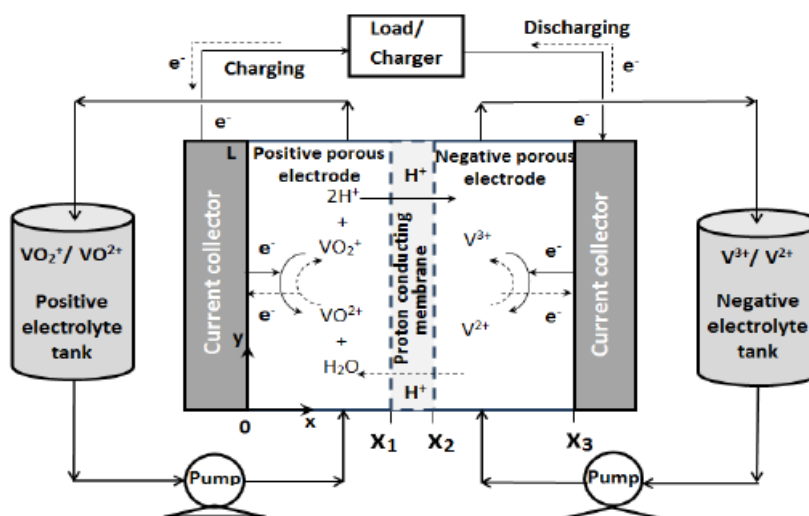
Figure 2.5: Shematic Structure of a Redox-Flow Battery, from [28]

rather than between an electrolyte and an electrode. These electrolytes are stored in two different tanks, separated by an Ion Exchange Membrane (IEM) that enables the transport of inert ions, closing the electric circle. During the discharge mode, the anolyte solution flows through a porous electrode and reacts to generate electrons, which flow through the external circuit [29]. During the charge, the flow of the electrons is reversed: oxidation occurs in the catholyte and reduction in the anolyte.

$$A^{2+} + C^{2+} \longleftrightarrow A^{+} + C^{3+} \tag{2.4}$$

2.3.3.1 Redox-flow chemistries

With advances in RFB research, different redox-flow chemistries have been studied. These batteries can be part of four different groups, based on their electrolyte composition, which includes their solvents (water or organic solvents) and their redox-active materials (aqueous metal-based or nonaqueous metal-based). Aqueous metal-based RFB uses water-based electrolytes with metal ions (such as iron, zinc or vanadium) as redox-active materials. These ions can be cycled between different oxidation states to store and release energy. [30]

The most promising RFB system is the Vanadium Redx-Flow Battery (VRFB). Vanadium is a chemical element with a huge number of important industrial applications. In these batteries, the liquid electrolyte is stored in tanks that use vanadium redox couples [31]. The chemical reactions between them are followed by the interchange of hydrogen protons through the ion exchange membrane. This is illustrated by the following chemical reaction:

$$V^{2+} + VO_2^{+} + 2H^{+} \longleftrightarrow VO^{2+} + V^{3+} + H_2O \tag{2.5}$$
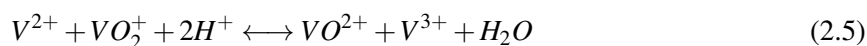
VRFB have special advantages when talking about ease of operation once the same electrolyte is used for both the positive and negative side. Their main disadvantage is related to their poor energy-to-volume ratio since they usually have a lower energy density than other types of batteries, which means they may require more physical space for the same energy storage capacity. In this sense, they're more suitable for large, fixed installations.

2.3.3.2 Battery models

Over the years, several proposals have emerged to model an equivalent electric circuit of VRFB. In this subsection, some of them will be presented.

Starting with the one presented in the paper [32] and shown on figure 2.6. Let's call it Equivalent Electric Circuit A (EEC A).
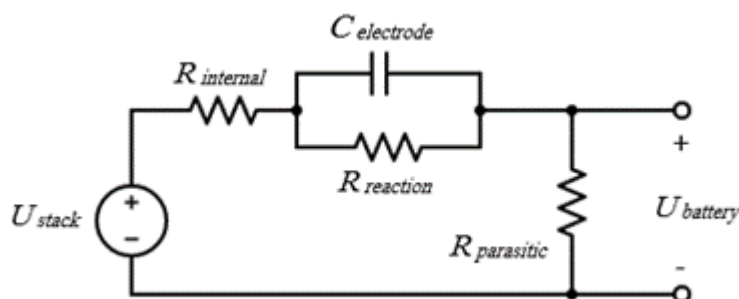
Figure 2.6: EEC A, adapted from [32]

It contains a voltage source that stands for the stack voltage, $R_{internal}$ and $R_{parasitic}$ resistors representing the losses (internal and external) that occur during the battery charging and discharging processes, and an RC banch holding $R_{reaction}$ and $C_{electrode}$.

The battery SOC is estimated dynamically and updates its value at each time step since its change is based on the power delivered or absorbed by the cell stack. The equation 2.6 defines it.

$$SOC = \frac{Current\ Energy\ in\ Battery}{Total\ Energy\ Capacity} = \frac{P_{stack}\ Time_{step}}{Energy\ Capacity}$$

$$= \frac{I_{stack}\ V_{stack}\ Time_{step}}{P_{rating}Time_{rating}} = I_{stack}\ V_{stack}\ C \tag{2.6}$$

This model takes into account the impact caused by the flow rate, flow pump losses and parasitic losses. However, its limitations lie in the fact that it does not consider self-discharge and cross-contamination effects. In addition, it also takes flow rate as static quantity, which increases the probability of making the model inaccurate for operations involving a dynamic flow rate.

In [33], a simple equivalent electric circuit is proposed (fig. 2.7) - let's say EEC B.

This circuit consists of a voltage source in series with an internal resistance ($R_{internal}$) corresponding to the effect of current excitation within the cell stack. It also displays two RC networks
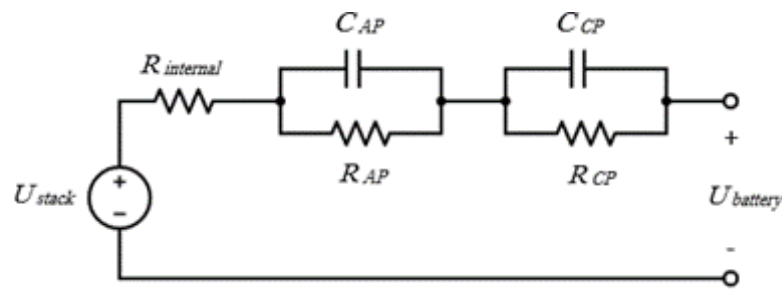
Figure 2.7: EEC B, adapted from [33]

representing the time-dependent dynamic activation and polarization concentrations.It is known that the number of RC networks is proportionally direct to the accuracy of the representation of the linear electrochemical processes within the battery, so this model is more accurate than the one previously analyzed.

Through the application of Kirchhoff's laws, it is possible to measure $U_{battery}$ (which represents the voltage at the battery terminals). The parameters corresponding to the RC branches can be estimated by applying the recursive algorithm of extended Kalman filter.

It is also important to address the limitations of the model (mentioned by the authors themselves in the paper) which include the fact that is does not consider the effects of practical parameters such as temperature, flow rate, or concentration/current density that influence the performance of the VRFB.

A modified version of circuit EEC B - EEC C is shown in figure 2.8 and has been proposed in paper [34].
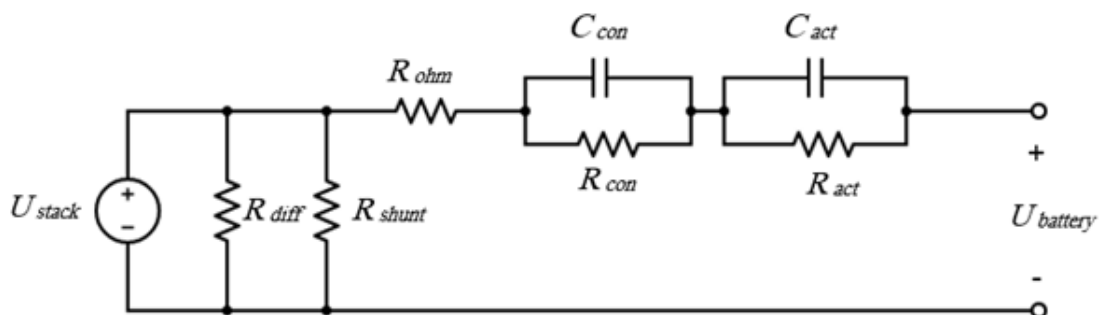
Figure 2.8: EEC C, adapted from [34]

The structure of this model is the same as the one presented previously, with the addition of two resistances, which signify the diffusion of vanadium ions across the ion exchange membrane. The combination of these two resistances (R_{diff} and R_{shunt}) is the equivalent self-discharge resistance.

Unlike the previous models, this one considers thermal effects. The model parameters are estimated through the Particle Swarm Optimization (PSO) technique. Its limitations include not

considering the dynamic flow rate during the charge/discharge processes, as in previous cases.

These three models discussed so far can be improved. Considering, for example, the effects of temperature (which directly influences the open-circuit voltage and battery capacity) it is possible to obtain better results in terms of battery performance since the battery capacity increases proportionally to the increase of temperature. The table 2.1 summarizes the considered effects in each model.

Table 2.1: Comparison between VRFB studied models

Model	Self-discharge consideration	Thermal effect consideration	Dynamic flow-rate consideration
EEC A	no	no	no
EEC B	no	no	no
EEC C	yes	yes	yes

Chapter 3

Methodology

This chapter focuses on the methodology that supports the optimization problem, widely discussed throughout this work. Initially, will be presented the battery models selected for this purpose, followed by the formulation of the problem in question and all that it entails, in this case, objective functions and respective constraints. The implementation of the problem in a programming language and all the associated challenges will also be discussed in the last section of the chapter.

3.1 Battery Modelling

In the next two subsections, the modelling of the two technologies used over the course of this work will be addressed in detail: the first one concerns the degradation model of a second-life battery, focusing on estimating the remaining life of it; then the model of the vanadium redox-flow battery, a promising technology in energy storage, is presented.

3.1.1 Second-life battery degradation model

While the reuse of portable Li-ion batteries has long gone unnoticed by the general public, the potential for reuse of electric car batteries, which has grown to be the market's dominating segment, is drawing increasing attention [35]. The rise in popularity of EV will naturally translate into an increase in recycled Li-ion batteries in the not-too-distant future. Undoubtedly, among the possible applications of second-life batteries, a possible reuse regarding energy storage in stationary systems stands out [36]. Therefore, it is essential to evaluate the degradation of the battery, both in its first and second life, mainly because there is literature that refers two different behaviors [37].

The aging model used in this subsection to account for battery degradation is based on the work of [38] and [39]. It should also be noted that the retired battery follows the same model as Lithium Iron Phosphate (which is currently the most widely used battery in the EV world [40]).

The number of annual battery cycles is related to: (i) E^{MILE}, which represents EV's daily driving mileage; (ii) EV's electricity consumption every 100 km, ε; and (iii) Q^{EV}, that stands for rated energy capacity of EV's battery.

A vehicle's daily driving mileage approximately follows a logarithmic normal distribution:

$$f_D(x) = \frac{1}{\sqrt{2\pi}\,\sigma_D\,x} \exp\left[-\frac{(\ln x - \mu_D)^2}{2\sigma_D^2}\right] \tag{3.1}$$

Based on equation 3.1, it is possible to calculate E^{MILE} :

$$E^{MILE} = 1.61 \cdot \exp\left(\mu_D + \frac{\sigma_D^2}{2}\right) \tag{3.2}$$

The annual charging-discharging cycle number of the battery is given by:

$$n_{battery} = \frac{365\,\varepsilon\,E^{MILE}}{100\,Q^{EV}} \tag{3.3}$$

Based on the above equations, the number of accumulated charge-discharge cycles of a Li-ion battery at the moment of its retirement from the EV can be estimated as:

$$n_{retire} = Y^{RETIRE} \cdot \left[\,n_{battery}\,\right] \tag{3.4}$$

where Y^{RETIRE} addresses the number of years of Li-ion battery serving the EV - this value was assumed to be 8 years. These charging-discharging cycles are responsible for battery degradation.

The maximum life cycle of a battery (n_{scrap}) is calculated based on the assumption it can no longer be used in an EV from the moment its capacity is less than 60% of its initial capacity. Based on this information and knowing that retired batteries with CRR (Capacity Retention Rate) below a certain value are no longer used, the CRR threshold was set to 0.6. Figure 3.1 illustrates the scenarios of possible reuse (or not) of batteries coming from EVs, based on their CRR value.
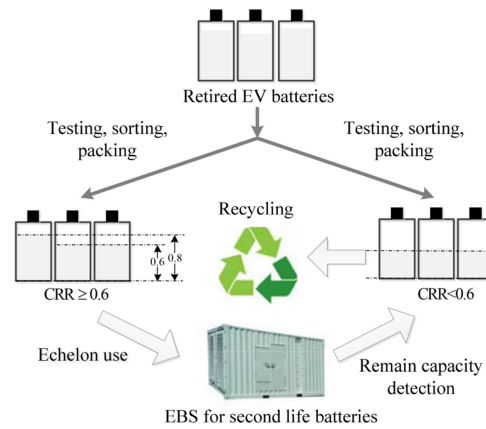
Figure 3.1: Evaluation process of retired EV batteries, from [39]

That said:

$$n_{scrap} = \left(\frac{Q_0(C) - 0.6}{\chi} \right)^{\tau^{-1}} \tag{3.5}$$

where Q_0 (C) is the initial capacity retention rate of the battery. χ and τ are constant parameters.

Subtracting equation 3.4 from equation 3.5, results the remaining life cycle of a battery at the time of its retirement:

$$n_{sec} = n_{scrap} - n_{retire} \tag{3.6}$$

It is necessary to consider the relationship between the depreciation rate of battery's CRR (R_c (n)) and its charging-discharging cycles:

$$R_c(n) = Q_0(C) - \chi \cdot n^{\tau} \tag{3.7}$$

Based on this, the capacity of the battery when it degrades from the CRR to the threshold can be determined by:

$$A_{SL} = A_{RATE} \cdot [\, R_c(n_{retire}) - 0.6 \,]$$

$$\Leftrightarrow A_{SL} = A_{RATE} \cdot [\, (\, Q_0(C) - \chi \cdot n_{retire}^{\tau} \,) - 0.6 \,] \tag{3.8}$$

where A^{RATE} is the capacity of the second-life battery.

Based on equations 3.6 and 3.8, the average depreciated capacity of the second life battery due to a full charging-discharging cycle (A^{FADE}) is projected to be:

$$A^{FADE} = \frac{A_{SL}}{n_{sec}} \tag{3.9}$$

In order to do life cycle calculations of a battery, it is necessary to first identify each half cycle, and the capacity at the end of each *kth* half charge-discharge cycle. A battery's full half cycle is completed between every two adjacent local extreme points. In this case, this is given by b_{update} (a variable that will be discussed in more detail later in this chapter). The DOD of every half cycle, d_k^{half}, is obtained as follows:

$$d_k^{half} = \frac{|b_{update}|}{E^{SL}} \tag{3.10}$$

It should be noted that E^{SL} stands for second life battery rated energy capacity. Battery's equivalent to a daily 100%-DOD, i.e., one complete daily battery discharge cycle, is represented by $N_{100}^{(eq,day)}$, being that:

$$N_{100}^{(eq,day)} = \sum_{k \in C} 0.5 \cdot (\, d_k^{half} \,)^{kp} \tag{3.11}$$

where *kp* is a constant ranging from 0.8 to 2.1. *C* stands for the set of half charge-discharge cycles.

The cost of battery degradation is, as expected, derived from its lifetime energy performance, number of cycles performed and, of course, the cost of the battery. EV battery degradation's cost is defined by the coefficient 3.12, derived from the work done on [41]:

$$c_{EV}^{deg} = \frac{c_{bat}}{e_{LTP}} \tag{3.12}$$

where c_{bat} is the cost of the battery (based on the information in [42]), and e_{LTP} is the lifetime throughput of the battery. This last parameter is calculated as:

$$e_{LTP} = \overline{DOD} \cdot n_{sec} \cdot E^{SL} \tag{3.13}$$

where $\overline{DOD}$ refers to battery's average depth-of-discharge.

Having said that, battery's degradation cost function (which is derived from this coefficient) is defined by:

$$c_d(t) = c_{EV}^{deg} \cdot b_{update} \tag{3.14}$$

All the parameters mentioned throughout this subsection are summarized in table 3.1, which also contains the value of each of them (values based on those presented in [38], [39] and [42]).

Table 3.1: Parameters used to calculate second-life battery degradation model

Description	Parameter	Value	Unit
constant parameter	μ_D	3.2	
constant parameter	σ_D	0.88	
electricity consumption every 100 km	ε	15	[kWh/ 100 km]
rated energy capacity of the EV battery	Q^{EV}	45	[kWh]
number of years of the battery serving the EV	Y^{RETIRE}	8	
initial retention rate of the battery	Q_0	0.9964	
constant parameter	τ	0.5	
constant parameter	χ	0.0067	
capacity of the 2nd life BESS	A^{RATE}	1.07e3	[Ah]
2nd life BESS rated energy capacity	E^{SL}	400	[kWh]
EV battery's cost per kWh	c_{bat}	120	[€/ kWh]

3.1.2 Vanadium redox-flow battery model

For the modelling of the vanadium redox-flow battery, the bucket model was used. In the state of the art, the pillars of this model were presented very briefly: an analogy is used to explain the basic functioning of a battery compared to a bucket (which stores electrical charge).

When the battery is connected to a device, it's as if the tap on the bucket is turned on - the water (electrical charge) starts to flow out of the bucket and into the device in question (resulting in

a decrease in the SOC of the battery). When the bucket is full of water, this represents the battery being fully charged (maximum SOC), and the electrical charge is stored in the battery. Figure 3.2 illustrates this operation.
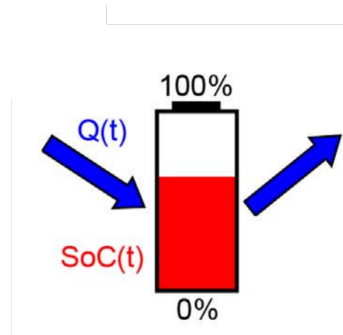
Figure 3.2: Bucket model representation, from [14]

The battery SOC is calculated in the traditional way (the ratio of the energy present in the battery to its nominal capacity) and varies, as expected, between 0 and 100%. In this model, there are no additional constraints to be met other than those related to the power limits of the battery itself. All these constraints are explained in subsection 3.2.2.

The main reasons for choosing this model for the representation of the vanadium redox-flow battery are again, the simplicity of it, and the visual stimulus - the visual representation of the buckets helps to create a clear mental image, valuable when it comes to retaining information and concepts.

3.2   Formulation of the optimization problem

An optimization problem is a type of mathematical problem where the goal is to find the best possible solution from a set of feasible options. This search entails the maximization or minimization of an objective function (the target of optimization) through the selection of variables, while considering constraints. The decision variables stand for the parameters that can be changed to accomplish the goal, whilst the constraints set a limit on the search space. The result is known as the optimum value. When the problems have more than one objective, we are faced with multi-objective optimization.

Data centers can be thought of as the "brains of the Internet", since they process, store and communicate all the data behind the services we rely on everyday (from social media to scientific computing). To achieve this, they use various IT devices, all of which require a significant amount of energy use. This used electricity turns into heat, that must be removed by using cooling equipment, that also consumes energy. All this energy consumption leads to carbon emissions – data centers depend on electrical grid that that are powered by a combination of energy sources (coal, natural gas, nuclear energy, oil, etc.); when these energy sources are used to generate electricity, burning fossil fuels releases large amounts of carbon dioxide into the atmosphere.

Most data centers rely on diesel generators for their energy storage, but with the pressure to reach carbon neutrality by 2030 there is a need for storage system solution. Note that the concept "carbon free" refers to running data centers on clean electricity that does not come from fossil fuels. At present, some companies already consider including distributed energy resources (such as PV generation and storage) in order to reduce their carbon footprint and increase its independence from the grid.

Batteries store energy, which can be release to power the individual components of the data center independently, without any use of readily available power.

The use of batteries in data centers is associated with the need to have a backup system in case there is an interference to the main power supply. This, however, is not the main objective of this problem - the work presented in the following sections aims to improve the self-consumption of the system with PV generation, and enable optimized management strategies through charging and discharging operations. To this purpose, mathematical models of both the second-life battery and the lithium battery (previously presented in section 3.1), and a set of constraints (discussed in subsection 3.2.2) were developed. The computational implementation of the model is described in section 3.3, where the methodology to obtain the chosen optimal solution is also explained. The subsequent problem is a day-head optimization problem that decides the battery charging and discharging operations for the next day. Thus, PV generation, HPC consumption and other values for the next day are only considered as predictions. In the scope of this work, these predictions are assumed to be correct.

3.2.1   Objective Functions

Savings in capital and operational costs are one way to describe the financial advantages of demand response utilizing batteries.

The most relevant goal of this problem passes by provide a tool that optimizes the battery operation in such a way that maximum economic value can be obtained from the total operation of the HPC system. Having said that, three objectives were defined for this problem: (i) minimize the energy costs from the operation of the system; (ii) minimize the cost of battery degradation; and (iii) minimize the cost associated with carbon intensity. All the constraints associated with the objective functions presented are set out in the next subsection.

Starting with function (i), its mathematical formulation is expressed in equation 3.15. $C_{buy}(t)$ represents the forecast electricity price purchased from the grid in €/kWh and $C_{sell}(t)$ the forecast electricity sale price to the grid, also expressed in €/kWh during the considered period. $P_{CC}^{in}(t)$ and $P_{CC}^{out}(t)$ represent power imported and exported from/to the grid, respectively (both expressed in kWh) over time. The variable $C(t)$ indicates the total cost of operation. Thus, it is understood that by minimizing the difference between electricity's purchase and sale cost, the total cost of the operation will also be minimized over the time horizon T_h (which is the same as maximizing

profits).

$$min \sum_{t=0}^{T_h} C(t) = min \sum_{t=0}^{T_h} \left[\left(C_{buy}(t) \cdot P_{CC}^{in}(t) \right) - \left(C_{sell}(t) \cdot P_{CC}^{out}(t) \right) \right] \qquad (3.15)$$

The formulation of the function associated with objective (ii) can be found in 3.16. As mentioned above, it meets the premise of minimizing the cost of degradation of the second-life battery, coming from an EV, over T_h. c_{EV}^{deg} relates to EV's battery degradation cost (as previously explained in subsection 3.1.1); b_{update} (t) represents the variation of battery energy caused by energy input or output at each instant of the time horizon (and will be explained with more detail in subsection 3.2.2).

$$min \sum_{t=0}^{T_h} c_d(t) = min \sum_{t=0}^{T_h} \left[c_{EV}^{deg} \cdot b_{update}(t) \right] \qquad (3.16)$$

Finally, the function associated with objective (iii) is found in 3.17. It aims to minimize the costs associated with carbon emissions during the period T_h. The variable $intensity_{CO2}$ (t) refers to the intensity of carbon emissions in g CO_2/ kWh. c_{CO2} represents the cost associated with one unit of CO_2, i.e. the cost in €/g of CO_2.

The cost of carbon emission in each time period t is then calculated by the product of the carbon emission intensity, together with the price associated with that emission and the amount of energy imported from the grid in that same time period. This function proves to be very useful as it can encourage the adoption of cleaner energy sources or the implementation of energy efficiency measures to reduce carbon emissions and mitigate the environmental impact associated with the use of energy from the electricity grid.

$$min \sum_{t=0}^{T_h} C_{carbon}(t) = min \sum_{t=0}^{T_h} \left[intensity_{CO2}(t) \cdot c_{CO2} \cdot P_{CC}^{in}(t) \right] \qquad (3.17)$$

3.2.2 Constraints

The constraints to be fulfilled while performing the economic minimization are provided by the mathematical model of the system and the data associated with each battery specifications (these are typical values for batteries, associated with the values considered in the project on which this dissertation was elaborated, and will be mentioned later in the next chapter).

Initially, it is necessary to ensure that the energy management in the battery is done properly. For this, a set of constraints were implemented, whose objective were simulate the behaviour of the battery when storing or releasing energy, based on the received power. These constraints also guarantee that the energy level in the battery is updated adequately, respecting the performance of the process. The most relevant decision variable of the problem is the charging/discharging power at a specific instant of time, $P_{ESS}(t)$.

The process starts by calculating the battery energy update, based on the initial energy contained in the battery ($b_{init\ energy}$) and the power affected by the throughput. The variable b_{update}

represents the variation of battery energy caused by energy input or output at each instant of the time horizon studied (T_h); the current battery energy at different time instants is given by b_{enegy}.

$$b_{energy}(t=0) \; = \; b_{init\ energy} \; + \; b_{update}(t=0) \tag{3.18}$$

When the battery is charging , b_{update} is given by the equation 3.19 and b_{enegy} by the equation 3.20. The charge efficiency (b_{eff}^{ch}) represents the efficiency of the energy storage process.

$$b_{update}(t) \; = \; P_{ESS}(t) \; \cdot \; b_{eff}^{ch} \tag{3.19}$$

$$b_{enegy}(t) \; = \; b_{enegy}(t-1) \; + \; b_{update}(t) \tag{3.20}$$

When the battery is discharging, b_{update} is given by 3.21 and b_{enegy} by 3.22. The discharge efficiency (b_{eff}^{dis}) represents the efficiency of the process of releasing energy to the external environment.

$$b_{update}(t) \; = \; \frac{P_{ESS}(t)}{b_{eff}^{dis}} \tag{3.21}$$

$$b_{enegy}(t) \; = \; b_{enegy}(t-1) \; + \; b_{update}(t) \tag{3.22}$$

In both cases, the value of b_{energy} was then calculated by summing $b_{init\ energy}$ with the result of b_{update} (for each specific case).

Battery's state of charge is calculated as the ratio between the remaining capacity in the battery at the desired time (b_{energy}) and the nominal battery capacity ($b_{capacity}$). Then, this value is multiplied by 100, in order to obtain the result in %. All this operation is showed in 3.23. In the context of the problem, this "desired time" refers to any instant within the time horizon T_h. SOC^{min} and SOC^{max} represent the minimum and maximum, respectively, charging levels in order to prevent overdischarge and overcharge (and assume different values depending on the technology of battery concerned), as depicted in 3.24.

$$SOC(t) \; = \; \frac{b_{energy}}{b_{capacity}} \; \cdot \; 100 \tag{3.23}$$

$$SOC^{min}(t) \leq \; SOC(t) \leq \; SOC^{max}(t) \tag{3.24}$$

In the context of energy management and storage in batteries, it is essential to ensure proper control of that energy flow during battery's charging and discharging process.

That said, constraint 3.25 aims to ensure that the charging and discharging power of the battery does not exceed the predefined maximum limits, that are determined based on the technical specification of each battery - defined by b_{max}^{pch} for maximum charging power, and b_{max}^{dis} for maximum

discharging power.

$$b_{max}^{pch}(t) \leq P_{ESS}(t) \leq b_{max}^{dis}(t) \tag{3.25}$$

One of the most important constraints of the problem lies in 3.26 as an equality constraint. Here, is calculated the net load (P_{load}^{net}), i.e., the difference between the total load coming from the HPC operation (P_{load}) and the total system generation at each point of the time horizon (P_{PV}^{gen}). It also adds the charging/discharging power of the battery, P_{ESS} at each instant. Essentially, this constraint ensures that the power balance is maintained at each time instant t (contained in the time horizon T_h).

$$P_{load}^{net}(t) = P_{load}(t) - P_{PV}^{gen}(t) + P_{ESS}(t) \tag{3.26}$$

By limiting the amount of energy that is sold (P_{CC}^{out}) or bought from the grid (P_{CC}^{in}), it is guaranteed the stability and safety of the electrical system, avoiding overloads. Both these parameters are limited in relation to P_{CC}^{limit}, the limit power for transactions at the Point of Common Coupling (which acts as a maximum contracted grid connection power).

$$P_{CC}^{in}(t) \leq P_{CC}^{limit} \tag{3.27}$$

$$P_{CC}^{out}(t) \leq P_{CC}^{limit} \tag{3.28}$$

In addition, it is also essential to ensure that no power is simultaneously imported or exported from or to the grid. Motivated by this, constraints 3.29 and 3.30 were formulated. It guarantees that, if there is power being imported (P_{CC}^{in}), there is no power being exported (P_{CC}^{out}) and vice-versa.

$$P_{CC}^{in} > 0 \quad \Rightarrow \quad P_{CC}^{out} = 0 \tag{3.29}$$

$$P_{CC}^{out} > 0 \quad \Rightarrow \quad P_{CC}^{in} = 0 \tag{3.30}$$

In the following section, these constraints will be mentioned again when explaining their algorithm for therefore implementation in the developed code, providing a complete overview of how to optimize the operation of the energy storage system.

3.3 Implementation

Throughout the development of this work, some of the optimization objectives that were proposed, do not allowed a linear approach (such as the degradation of batteries). As mentioned in chapter 2, that degradation process is non-linear, so the optimization strategy to be adopted has to satisfy this criterion. Solving non-linear problems can be quite challenging - there may, for example, be

numerous local optima that are not necessarily the global optimum. A certain sensibility is also required in the choice of the method to be used, initial parameters and possible assumptions since they can significantly influence the accuracy of the solution. The attempt at linearization is not always adequate or even feasible due to a panoply of reasons, among the most significant being the possible loss of information/inaccurate representation of the original problem, as well as the computational complexity that can derive from it - the introduction of linear constraints or terms can significantly increase the complexity of the final solution, ultimately requiring significant computational resources.

Therefore, search and optimization algorithms are typically designed utilizing certain heuristics that, despite lacking strong mathematical underpinnings, are good at arriving at an approximation of the solution in a reasonable amount of time in order to address such issues practically.

3.3.1 Metaheuristic methods

Metaheuristics are a class of optimization algorithms that provide general frameworks for solving complex optimization problems. Most of these methods are based on principles of biological evolution and seek to emulate natural processes. The optimal sizing and placement of batteries are easier to solve through the use of these methods. In the subsection below, some of these algorithms will be covered, with particular emphasis on EPSO, the algorithm used for the development of the work associated with this dissertation.

3.3.1.1 PSO

Particle Swarm Optimization (PSO) is a metaheuristic optimization algorithm whose main idea is an analogy to the behaviour of swarms of insects, flocks of birds or shoals, which have the movement influenced by inertia, memory and cooperation. The principle of operation, centers on the fact that in each iteration there is a set (swarm) of solutions, called "particles", which from one iteration to the next move with a certain velocity [43]. Considering X_i as a particle in each iteration, V_i represents the velocity of said particle. The movement rule is defined as:

$$X_i^{new} = X_i + V_i^{new}$$

$$\Leftrightarrow \quad X_i^{new} = X_i + (X_i - X_i^{old}) + Rnd_1 w_1 (b_j - X_i) + Rnd_2 w_2 (b_g - X_i) \tag{3.31}$$

The introduction of the term R_{ndx} in 3.31, stands for a number in [0, 1] sampled from a uniform distribution (this introduction is characteristic of all PSO models [44]). As mentioned earlier, there are three major factors that influence the motion. Starting by inertia - the first term tends to project the particle in the same direction it was going; memory - the second term projects the particle to its best past, which manipulates the search process to return to the most promising region already visited by the particle so far; and finally cooperation - the third term that "pushes" the particle to

the most promising region discovered by the whole swarm, coinciding with the most promising location globally [45]. Figure 3.3 summarizes the concepts covered so far.
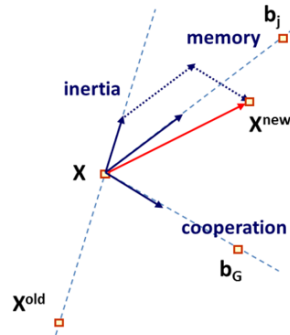
Figure 3.3: The idea behind PSO, from [44]

Thus, 3.3 makes it clear that new particle is generated from a composition of the differences of 3 previously discovered points to the current particle position X.

It is extremely important to note that PSO is an iterative algorithm, however not evolutionary, since there is no "selection" operator or competition between individuals.

Problems associated with this algorithm include instability and difficulty of convergence, as numerous trials may be required to find the weights (w_1 and w_2) for each problem, and the need to distinguish between global exploration (which refers to the capacity to seek for potential solutions in new areas of the search space) and local exploitation (which refers to the capacity to focus on known regions of the search space that are promising in terms of optimization) [46].

3.3.1.2 EPSO

Evolutionary Particle Swarm Optimization (EPSO) algorithm grew out of the combination of PSO with conceptual evolutionary search strategies, and emerged with the aim of improving PSO's weaknesses.

Evolutionary computation emerged from the idea of imitating the mechanisms of biological evolution. The general evolutionary process over a reproducing population relies on three major conditions: diversity, selection mechanism and transmission mechanism. Figure 3.4 illustrates evolutionary theory in the light of what Darwin's ideas.

The idea behind this algorithm is to introduce a self-adaptive scheme in the introduction of the weights of the various components. The scheme presented in figure 3.5 shows the fit of evolutionary theory in the concrete case of EPSO.

The particle movement rule is defined as:

$$X_i^{new} \; = \; X_i + V_i^{new}$$
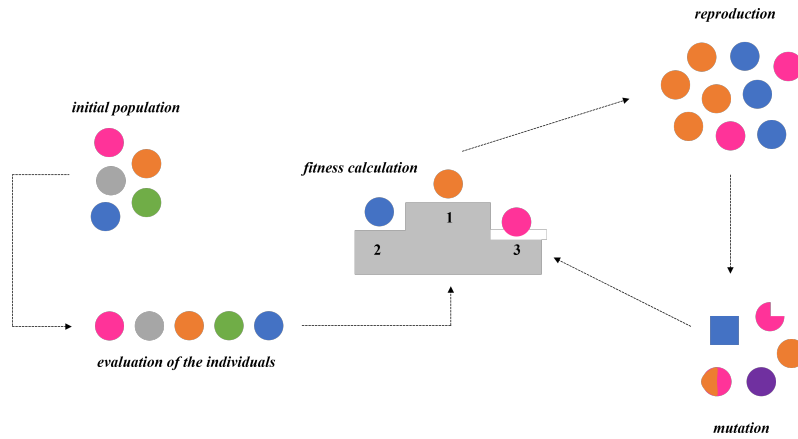
Figure 3.4: Darwin's evolution theory, adapted from [47]
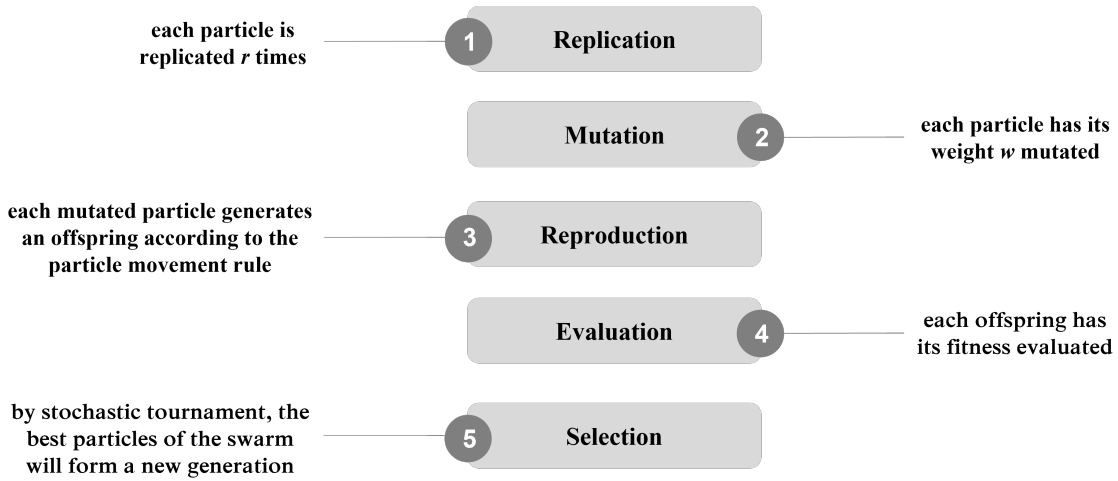
Figure 3.5: The idea behind EPSO, adapted from [48]

$$\Leftrightarrow \quad X_i^{new} = X_i + \tilde{w_I}(X_i - X_i^{old}) + \tilde{w_M}(b_i - X_i) + \tilde{w_C}(b_g - X_i) \tag{3.32}$$

being,

$$\tilde{w_{\{I,M,C\}}} = w_{\{I,M,C\}} + \tau N(0,1) \tag{3.33}$$

$$\tilde{b_g} = b_g(1 + \tilde{w_b}N[0,1]) \tag{3.34}$$

with $\tilde{w_b}$ representing the local exploitation factor, and being defined as:

$$\tilde{w_b} = w_b(1 + \tau'N[0,1]) \tag{3.35}$$

Note that the variables τ and τ' are fixed weights, viewed as learning parameters. Read "~"

as "subject to mutations". Thus, each of the weights is subject to mutations, which causes the recombination operator to evolve.

The process starts by divide the variables into object parameters (X variables) and strategic parameters (w weights) [46].

Equation 3.32 shows clearly that are needed four contribution to create an offspring: his direct ancestor (X_i), the ancestor of its ancestor (X_i^{old}), a possibly distant past best ancestor (b_i) and a current global best known to this particle (b_g) [46]. Also, the sum of the weights multiplying each ancestor is 1.

The movement rule is illustrated in 3.6. The 4 ancestors mentioned above are highlighted.
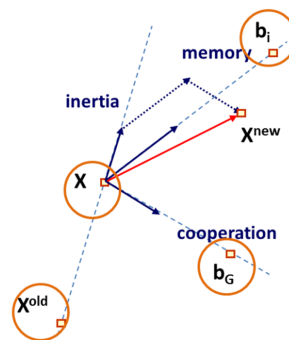
Figure 3.6: Reinterpretation of EPSO's movement rule, from [44]

3.3.1.3 Conclusions on EPSO and PSO

PSO and EPSO algorithms were explained in a very detailed way. As a summary, the main differences and advantages between them can be highlighted:

- evolutionary approach: unlike EPSO, PSO is not an evolutionary algorithm since it has no "selection" operator or competition between individuals

- computing complexity: EPSO can be more computationally challenging due to the need to perform evolutionary operations (selection and recombination), which PSO does not require

- copulation diversity: the candidate solutions population that EPSO keeps, changes across generations, which increases the chances to find better solutions

That said, and after the literature confirmed the efficiency of EPSO for solving problems associated with power systems (as in [49]), this algorithm was chosen to solve the problem in hands.

3.3.2 Python libraries and implementation

The code object of this work was developed in Python. The versatility and simple syntax of this programming language were relevant advantages. In addition, Python has numerous importable

libraries that add specific functionalities to it, some of them used throughout the course of this dissertation, and now summarized in 3.2.

Table 3.2: Used libraries in Python and their respective purpose

Library	Utilization
Pandas	data analysis and manipulation of tabular structures
PVlib	generation of synthetic data associated with photovoltaic power generation
Numpy	numerical computation and mathematical operations
Matplotlib	creation of graphics and consequent visualization of results
Datetime	handling and calculating dates and times efficiently

Initially, EPSO parameters were defined in a dictionary called *input_opt*. The information contained in this dictionary includes the maximum number of generations (200), number of particles in the swarm (96), mutation rate (0.4) and communication probability (0.8).

Following this, it was necessary to set decision variable bounds, i.e. define the maximum (x_{max}) and minimum (x_{min}) positions for the swarm particles in space. Both variables are vectors, each with the same size as the time horizon, previously initialized, and then filled in: the maximum position is equal to the maximum charging power of the battery, and the minimum position equal to the symmetric value of the maximum discharging power of the battery (both values defined in tables 4.1 and 4.2).

After this, it was required to establish the swarm. It is already known that the swarm contains 96 particles, and, in the proposed model, each particle represents a possible solution to the problem. The best global solution found so far is stored in a list, *g_best_pos* (as expected, initially this list is empty because no solution has been found yet). A variable called *g_best_pos_fit* is also created and will be used to track the fitness value of the best solution found so far. At its creation, it is assigned the highest possible value in order to ensure that any fitness value is lower than the initial value, updating the best overall solution. It is important to note that the lower the fitness value, the better the solution - since it is a metric that reflects the performance of the solution relative to the goal, a lower fitness value indicates a solution closer to the goal. Using the "*evaluate*" function, the fitness of the particle is evaluated in relation to the objective function f. After that, a comparison is made between the fitness of the current particle and the best global fitness found so far: if the former proves to be a better solution, the value of *g_best_pos_fit* is then updated to that, as well as changing the value of *g_best_pos* for the position of the particle in question.

This is followed by some additional calculations in order to calculate the SOC, power balance, etc. of the best solution (basically all the parameters mentioned in subsection 3.2.2). These are stored in another dictionary called outputs that is returned as the final result of the optimization, along with the optimal solution and its status, i.e. whether it is feasible or non-feasible (note that it is enough to disrespect only one constraint imposed by the problem for the solution to be automatically non-feasible).

Run_epso is the main function to run iterative EPSO algorithm. It starts by initializing a counter (called *i*), relative to the iteration in question, and creates a list *g_best_pos_fit_hist* that

will serve as a history of *g_best_pos_fit* values. It also makes a copy of the swarm at the beginning of each iteration so that the original swarm is not changed during iteration. Next, a loop is run through the swarm that mutates weights and updates velocities, positions and fitness. In the final part of this function, another loop is run through swarms and update particles and global best position: if the fitness of the mutated particle is better than that of the original, *g_best_pos* and *g_best_pos_fit* are updated. This process is repeated until *max_gen*. At the end, *g_best_pos*, *g_best_pos_fit* and *g_best_pos_fit_hist* are returned.

Afterwards, a function *f* was defined, in which the vector v[t], containing the best values of the power in the battery throughout the day, was created. Within this function, the weights associated with each of the objective functions are also defined: in this case, an equal weight was consider for each function.

Finally, a function called *check_constraints* was also computed with the purpose to add penalties for violated constraints. The penalty in question was defined as *pen* in the code and initialized to 0, taking the value of 1E+4 in each case of unfulfilled constraint. This value was so high to ensure that in case the constraints are not strictly obeyed, there was a significant impact on the objective function and, consequently, on the final result. It is important to note that the values of the vector v[t] (which, as mentioned before, represent the values of the power in the battery throughout the day) were divided into 2 vectors: v_{sl}[t] with the first 24 values of v[t], which concern the daily charge/discharge of the second life battery; and v_{vr}[t] corresponding also to the daily charge/discharge, but of the vanadium redox-flow battery. The constraints implemented here are those discussed in subsection 3.2.2. At the end, the mathematical calculation of the objective functions is carried out, also based on the one mentioned in subsection 3.2.1 .

The flowchart presented in 3.7 provides a clear and concise summary of the implemented code, giving an overview of the execution process and the key steps involved.
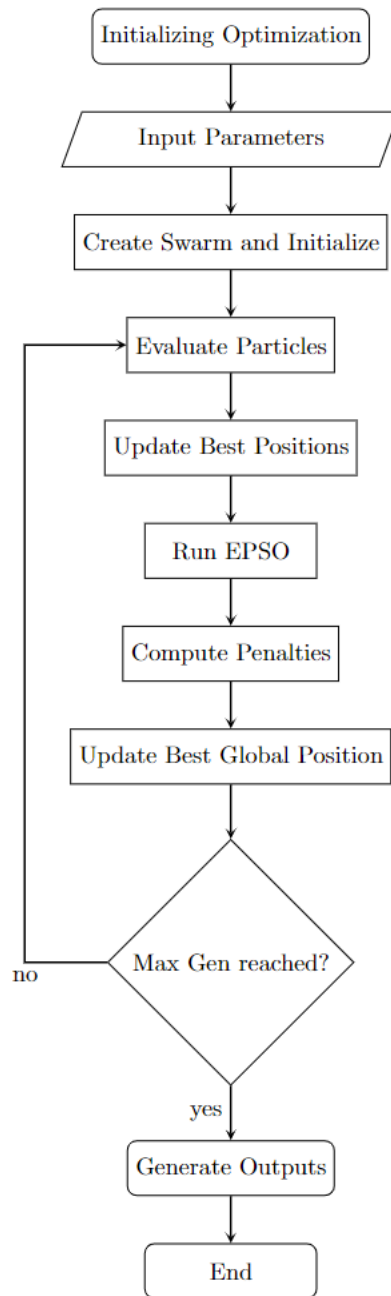
Figure 3.7: Flowchart summarizing the steps of the implemented code

Chapter 4

Case Study

To obtain results that can be critically analyzed, the methodology presented in the previous chapter was applied to a case study, which represents a possible real case to apply the concepts discussed.

4.1 Description

The case of study goes through energy management and storage to be implemented around the Deucalion supercomputer, optimizing its energy consumption and thus, the attempt to reduce the carbon emissions associated with its activity.

Deucalion (in figure 4.1) is a petascale supercomputer, capable of executing the maximum performance of 10 Petaflops, in other words, 10 million billion calculations per second. Its operation relies primarily on electricity from renewable sources, utilizing intrinsic capacity brought about by the installation of solar photovoltaic panels, storage in second-life EV batteries and in vanadium redox-flow batteries, and electricity from the grid (when its electricity is from renewable sources). This HPC system will be installed at FCT's Minho Advanced Computing Center (MACC), with coordinates 451.45088º N (latitude) and -8.29366º W (longitude).

Figure 4.1: Deucalion supercomputer, from [50]

In order to achieve the proposed objectives, two different technologies have been implemented: second-life batteries from EV, and vanadium redox-flow batteries (their models have been explained in detail in the previous chapter).

4.2   Specific inputs

4.2.1   Battery data

The values of each specific parameter for both second life and vanadium-redox flow batteries are listed in the tables 4.1 and 4.2, respectively. These are typical values for batteries, associated with the values considered in the project on which this dissertation was elaborate.

Table 4.1: Specific parameters' values for the second life battery

Description	Parameter	Value	Unit
nominal capacity	$b_{capacity}$	1500	[kWh]
initial energy content	b_{energy}	750	[kWh]
min. state of charge	b_{min}^{SOC}	20	[%]
max. state of charge	b_{max}^{SOC}	80	[%]
max. charge power	b_{max}^{pch}	300	[kW]
max. discharge power	b_{max}^{pdis}	300	[kW]
constant charge efficiency	b_{eff}^{ch}	90	[%]
constant dicharge efficiency	b_{eff}^{dis}	90	[%]

Table 4.2: Specific parameters' values for the vanadium redox-flow battery

Description	Parameter	Value	Unit
nominal capacity	$b_{capacity}$	500	[kWh]
initial energy content	b_{energy}	250	[kWh]
min. state of charge	b_{min}^{SOC}	5	[%]
max. state of charge	b_{max}^{SOC}	95	[%]
max. charge power	b_{max}^{pch}	100	[kW]
max. discharge power	b_{max}^{pdis}	100	[kW]
constant charge efficiency	b_{eff}^{ch}	80	[%]
constant dicharge efficiency	b_{eff}^{dis}	80	[%]

4.2.2   Electricity prices and carbon intensity

The information on electricity prices and carbon intensity was provided by INESC TEC and subsequently properly processed and filtered for the year 2022. This filtration was performed by manipulating Dataframes, a structure of the Pandas package of Python. The code used to process this data is shown in figure 4.2.

```python
1   import pvlib
2   import pandas as pd
3   import numpy as np
4   import datetime as dt
5   import time
6
7   carbon_intensity = pd.read_csv(r'C:\Users\listr\Desktop\Sustainable
    ↪  HPC\Sustainable HPC
    ↪  Liliana\opttool\core\module\helpers\carbon_intensity.csv')
8
9   carbon_intensity['datetime'] = pd.to_datetime(carbon_intensity['datetime'])
10
11  carbon_filtered = carbon_intensity.loc[carbon_intensity['datetime'].dt.year ==
    ↪  2020]
12
13  carbon_filtered['datetime'] =
    ↪  carbon_filtered['datetime'].mask(carbon_filtered['datetime'].dt.year ==
    ↪  2020,
14                             carbon_filtered['datetime'] +
                               ↪  pd.offsets.DateOffset(year=2022))
15
16
17  market_prices = pd.read_csv(r'C:\Users\listr\Desktop\Sustainable
    ↪  HPC\Sustainable HPC Liliana\opttool\core\module\helpers\market_prices.csv')
18
19  all_dates = pd.date_range(start='2022-01-01 00:00', end='2022-12-31
    ↪  23:00',freq='H')
20
21  all = all_dates.strftime('%Y-%m-%d %H:%M:%S')
22
23  market_prices['datetime'] = pd.to_datetime(market_prices['datetime'])
24
25  price_filtered = market_prices.loc[market_prices['datetime'].dt.year == 2022]
26
27  price_filtered = price_filtered.resample('H', on =
    ↪  'datetime').mean().reindex(all).fillna(method='backfill').reset_index()
28
29  price_filtered.rename(columns={'index': 'datetime'}, inplace=True)
```

Figure 4.2: Code implemented to process data from the market prices and carbon intensity

It should be emphasized that, as can be seen in 4.2, the information relating to carbon intensity have been filtered for 2020. This was due to a question of time and logistics: the available data (in this case, for 2020) was used, and the same behavior was assumed for 2022, the year under study.

After this, two graphics were made in order to obtain a visual representation of the treated data. The amount of information available makes the analysis unintuitive and unwieldy. In order to combat this behaviour, the choice was made to transform the hourly data for both cases into a monthly average data. Figures 4.3 and 4.4 illustrate then year scenario for electricity's monthly average market prices, and monthly average carbon intensity for 2022, respectively.
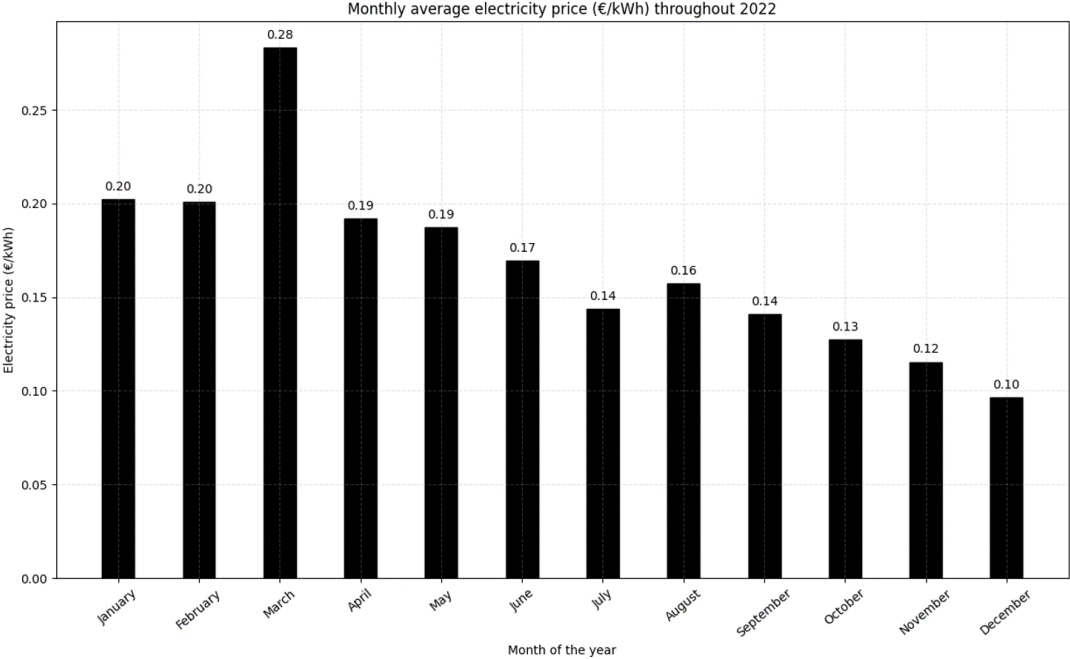
Monthly average electricity price (€/kWh) throughout 2022

Figure 4.3: Electricity's market average prices over 2022

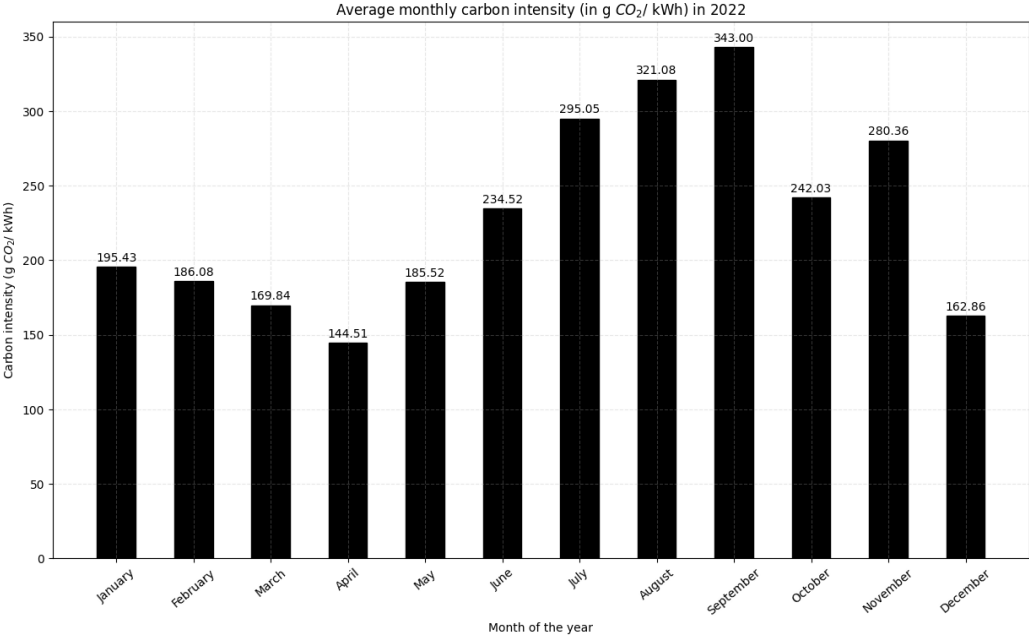Average monthly carbon intensity (in g CO_2/ kWh) in 2022

Figure 4.4: Average montlhy carbon intensity over 2022

4.2.3 PV generation

Data regarding PV generation throughout the year was produced synthetically using the Python PVlib library, and via PVGIS (Photovoltaic Geographical Information System). The function *pvlib.iotools.get_pvgis_hourly* gets hourly photovoltaic energy generation data from PVGIS.

The parameters provided to the function are the geographic coordinates of the location (latitude and longitude), the start and end year, the inclination and azimuth of the location where the solar panels will be installed, and the peak power of the panels. The values for each of these inputs are summarized in table 4.3.

Table 4.3: Specific parameters' values used on the PV generation function

Parameter	Value	Unit
latitude	451.45088	[º N]
longitude	-8.29366	[º W]
surface tilt	30	[º]
peak power	1000	[kWp]
star year	2015	
end year	2015	

Looking at the table, it can be seen that the panels will be installed with 30º tilt and 0º azimuth, which means that they are tilted upwards and facing north, respectively. After this, the data related to PV power generation is converted to more common units (from 100 W/m^2 to 1 kWh/m^2), resampled by hour, and the year is changed from 2015 to 2022 (considering that the PVGIS does not cover the year 2022, a random year was used and equal behavior was assumed for the target year.), for further analysis. The code displayed in 4.5 shows the process designed to obtain PV generation values.

```python
import pvlib
import pandas as pd
import numpy as np


pv_gen = pvlib.iotools.get_pvgis_hourly(41.45088, -8.29366, start=2015,
        end=2015, surface_tilt=30, surface_azimuth=0,
        pvcalculation=True, peakpower=1000)


pv_gen = pv_gen[0]['P'].apply(lambda x: x/100)


pv_gen = pv_gen.resample('H').mean()


pv_gen = pd.DataFrame(data={'datetime': pv_gen.index, 'pv': pv_gen.values})


pv_gen['datetime'] = pv_gen['datetime'].mask(pv_gen['datetime'].dt.year == 2015,
                    pv_gen['datetime'] + pd.offsets.DateOffset(year=2022))

```

Figure 4.5: Code implemented to generate PV values

After the implementation of the code, PV generation values were obtained for each day of the year 2022. This information was handled appropriately, and the 4.6 graphic shows the monthly sum of this data.
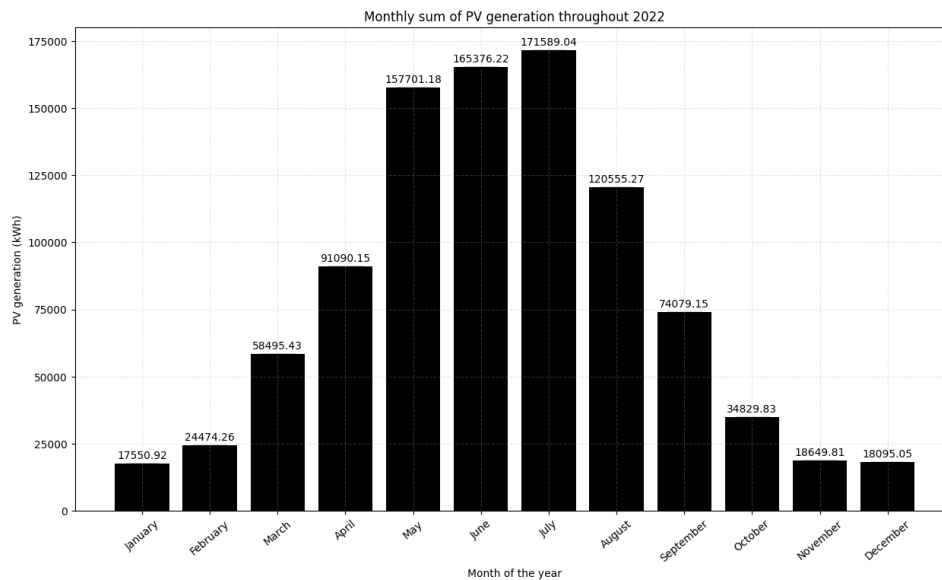

Figure 4.6: PV generation over 2022, for the local correspondent to the previous indicated coordinates

As expected, PV generation was higher in the summer months, as a result of the increased intensity and duration of sunlight in that season. These results highlight the importance of seasonality in solar energy generation and emphasise the need for energy storage or complementary energy sources to meet demand during the months of lower generation.

4.2.4 Supercomputer load

In order to assess the energy requirements of the supercomputer and model its power consumption, it was delevoped a function (showed in figure 4.7) called *gen_load*, which then serves the purpose of generating a consistent load profile for the supercomputer. It does so by taking into account the predefined average utilization rate. The function receives four different parameters: the nominal value of the supercomputer's load (*nominal*), the average utilization rate of the supercomputer (*avg_util*), the load value when the supercomputer is not being used (*idle*) - which for this problem, was assumed to be 0.25 (note that this value is presented as a nominal fraction, and corresponds then to 25% of the load) - and the total number of hours for which the load profile should be generated (*full_time*). Given that the operation is designed on an annual basis, the variable *full_time* takes the value 8760 (corresponding to the number of hours in a year).

In line 22 of figure 4.7 stands the formula used to calculate the value of the supercomputer load in each hour: it can be seen that this corresponds to the product of the supercomputer load when it

is in use with average utilization rate (transformed from percentage into a fractional value), added to the product of the supercomputer load when it is not in operation with the average utilization rate and the nominal idle value.

After this, values are assigned to the missing function inputs: the nominal value of the supercomputer load (*nominal*) takes the value of 1000 kW, and the average utilization rate (*avg_util*) is taken as 85% (this value comes from the expectation that the system will have a very high actual utilization, possibly even higher than 85%.).

Finally, through the *gen_load* function, whose objective is to generate load data for a given period of time (in this case, 1 year) based on the daily profile provided, and adding randomness to the daily values every hour, the load profile of the supercomputer was then generated.

In order to be able to present the results obtained as clearly as possible graphically, it was decided to plot the supercomputer's monthly energy consumption figures for each month of the year. These are illustrated in figure 4.8.

```python
import numpy as np
import datetime as dt
import time

def gen_data(daily_profile, daily_var, timestep_var, full_time=8760,
   l_bound=-1E+50, u_bound=1E+50):

    np.random.seed(42)

    daily_delta = np.repeat(np.random.normal(0, daily_var, int(8760/24)), 24)

    timestep_delta = np.random.normal(0, timestep_var, int(8760))

    profile = [float(x * (1 + d + t)) for x, d, t in zip(daily_profile *
        int(full_time / 24), daily_delta, timestep_delta)]

    new_profile = np.clip(np.array(profile), l_bound, u_bound)

    return [float(x) for x in new_profile]


def gen_load(nominal, avg_util, idle=0.25, full_time=8760):

    load = (avg_util / 100) * nominal + (1 - avg_util / 100) * idle * nominal

    return [load for _ in range(full_time)]

load = gen_load(1000, 85)

p_load_full = gen_data(load, 0.02, 0.0025, full_time=24, l_bound=700,
    u_bound=1000)
```

Figure 4.7: Code implemented to generate supercomputer's load
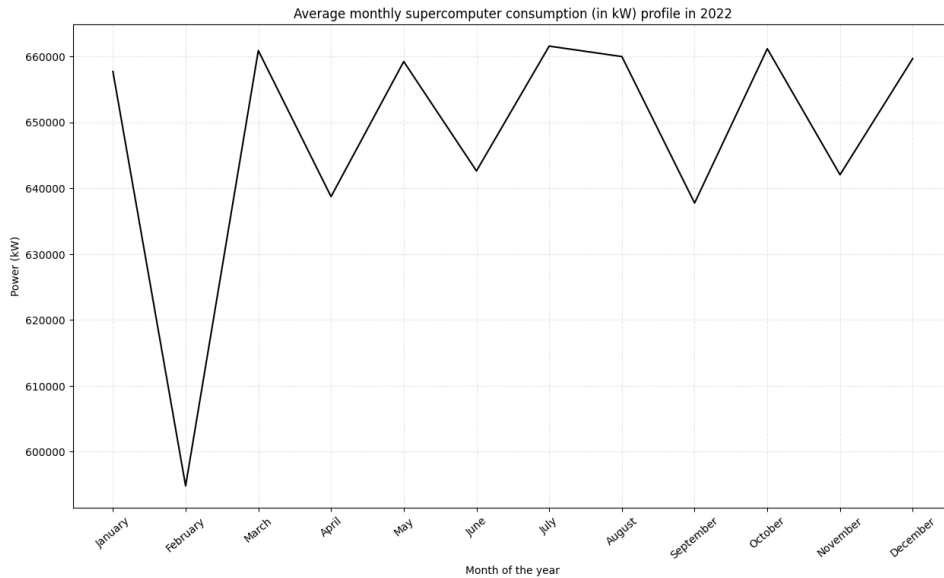
Figure 4.8: Average monthly supercomputer consumption profile in 2022

4.3 Results and discussion

This section will analyze the results obtained, based on the methodology described and the inputs presented above.

Initially, the optimization was run for a long-term scenario, where the simulation was performed for a representative month, covering seasonal variations and patterns that can be replicated for the optimization behavior for a typical year. Subsequently, and in search of a more detailed analysis, the optimization was conducted for a random day in the year 2022.

The results of both scenarios are described in the next subsections.

Before that, subsection 4.3.1 will present the results related to the modeling of the second battery in the context of the transition from first to second life.

4.3.1 Li-ion battery: from first to second life

Using the formulas previously presented in chapter 3, together with the values in table 3.1 for the specific parameters of second life batteries, the annual number of charge and discharge cycles of the battery was calculated to begin with. Next, the average depreciated capacity of a second-life battery over a full charge/discharge cycle was obtained. Speaking of the battery operation when used in the EV, the daily driving mileage of the battery was calculated. The remaining capacity of the battery when it degrades to threshold was also estimated. The number of cycles the battery has done in the first life, number of maximum cycles to be done and number of cycles that can still be done in the second life have also been duly calculated.

Table 4.4: First-to-second life parameters of the Li-ion battery

Description	Parameter	Value	Unit
daily driving mileage	E^{MILE}	58.17	[km]
annual charging-discharging cycle number	$n_{battery}$	70.78	
number of accumulated cycles at retirement from the EV	n_{retire}	566.22	
max. life cycle	n_{scrap}	3500.40	
cycles that can still do in second-life	n_{sec}	2934.18	
remaining capacity when in degraded to treshold	A_{SL}	253.56	[kWh]
depreciated capacity due to a full ch-disch cycle	A^{FADE}	0.086	[kWh]

By looking at the table 4.4, the theory discussed above is proven: in fact, when an EV battery is retired, it still has a considerable number of cycles that can be done, hence the talk around reusing them.

In this specific case, the number of cycles that can be done in the second life of the battery corresponds to almost 80% of the maximum number of cycles that it can do in total, so it is extremely advantageous to use it for a possible application to the problem in question.

Regarding its degradation per complete charge or discharge cycle, this value proves to be low, which provides the possibility of so many complete cycles in the second life and agrees with what was mentioned in the previous paragraph, further reinforcing the idea of the plausibility of a second life for this battery.

4.3.2 Scenario 1: Optimization for a day in 2022

In line with the above, it started by running the optimization for a random day. In this case, the day chosen was 2022-01-24. In the search for a more thorough understanding of how a high performance system functions, the forecasting of an atypical day plays a crucial role. Focusing on only one day, randomly selected from the 365 days in a year, allows to examine how the system behaves under various and unpredictable conditions.

Starting with the examination of the second-life battery's activity, figure 4.9 illustrates the power variations during both its charging and discharging cycles over the course of the day. For further insights into these patterns, figure 4.10 offers a comparative view, incorporating the SOC data of the battery.

From the analysis of 4.10 it can be seen that its state-of-charge starts relatively close to the minimum value it can take. As the day goes on, the battery's state of charge increases until around 2pm, after which it drops, reaching almost the lowest possible value again in the last hour of the day.

Naturally, it can be seen that in the hours when the battery is charging (corresponding to the positive values of the bars) the SOC is higher and, naturally, in the periods when the battery is discharging (corresponding to the positive values of the bars), the SOC tends to be lower.

Note that the SOC is progressively increasing from midnight until 2 PM, indicating that the battery is charging. In contrast, the charge/discharge vector of the battery at these times does not
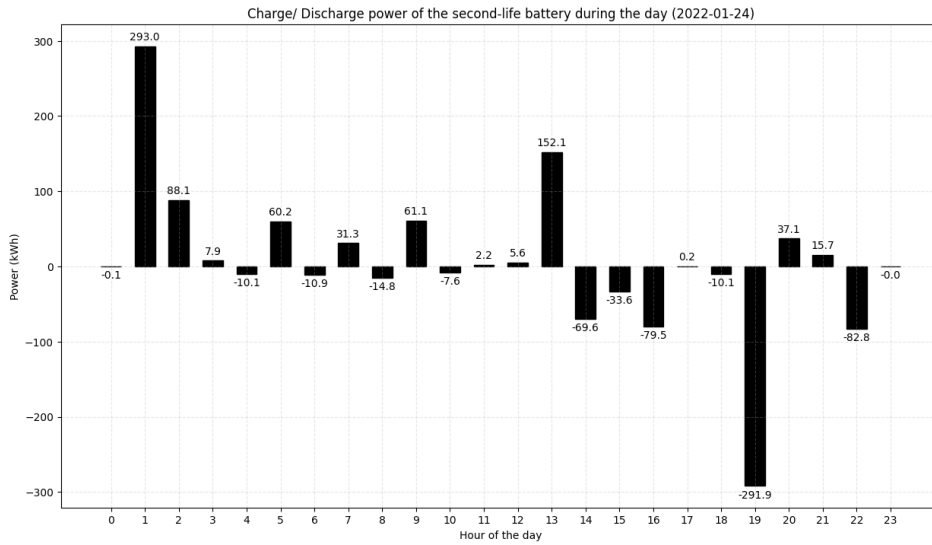
Figure 4.9: Charge/Discharge Power of the second-life battery during 2022-01-24
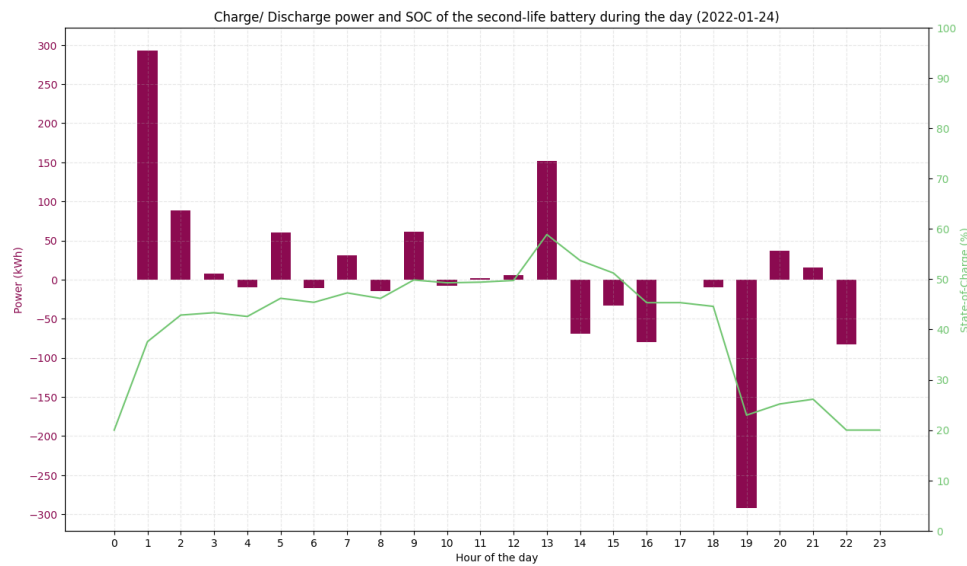
Figure 4.10: Charge/Discharge Power of the second-life battery and its SOC during 2022-01-24

show high discharges, suggesting that the energy generated by the PV system is being used to charge the battery. After 2 PM, the state of charge begins to progressively decrease until 11 PM, reaching a value very close to the minimum required by the battery (approximately 20%). The discharge values associated with this time indicate that the energy stored in the battery is being used for fuelling, resulting in a decrease in the SOC.

The talk about daily battery degradation, i.e. the analysis of $N_{100}^{(eq,day)}$ is also the subject of study. Graphic 4.11 shows this results.
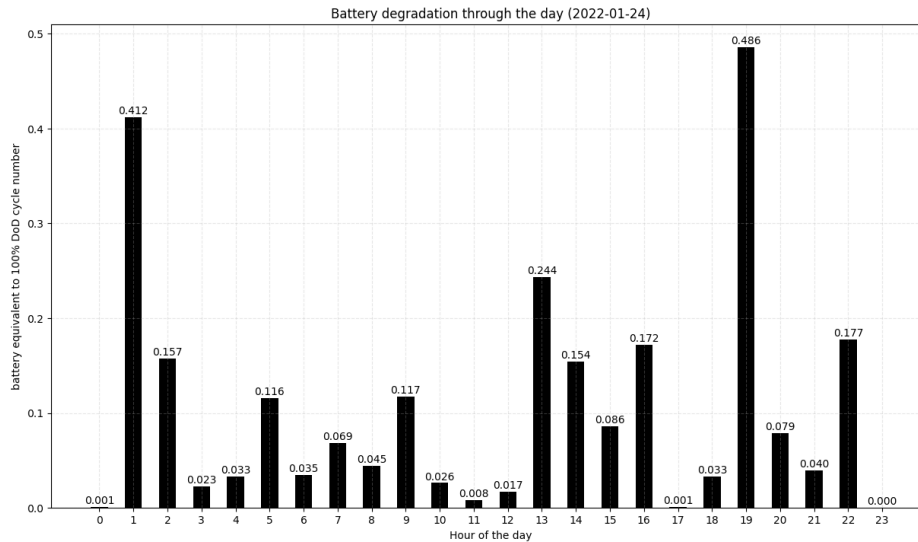
Figure 4.11: Second-life battery's degradation during 2022-01-24

As expected, the periods with the highest battery charge or discharge values correspond to the periods with the highest degradation values (highlights to 1 AM and 7 AM, corresponding to the highest charge and discharge power, respectively).

The cost of second-life battery degradation is dependent on the operation of the device (as expected, and mathematically proven in chapter 3). Graphic 4.12 shows the relationship between this variable and daily battery degradation.

Again, as antecipated, higher battery degradation corresponds to higher cost, not least because these variables are proportionally related. The maximum value reached (at 19 PM) is approximately 0.056 €/kWh. In that hour alone, the cost of battery degradation is approximately 84 €, (this value is obtained by multiplying the coefficient 0.056 €/kWh by the battery capacity). Thus, the weight that this degradation has in the financial balance of the problem becomes clear.

Let's now move on to look at the operation of the vanadium redox-flow battery. Similarly to what was done for the second life battery, we start by projecting the charge and discharge values of this battery, illustrated in 4.13.

It is noticeable that, compared to the second-life battery, this one has a slightly lower number of discharge periods. Nevertheless, there are quite sharp oscillations - for example, between midnight and 1 AM where it goes from discharging 91.7 kW to charging 1.4 kW.

The relationship between the charge and discharge of this battery and its SOC is shown in 4.14. Once again, everything behaves within the normal range.
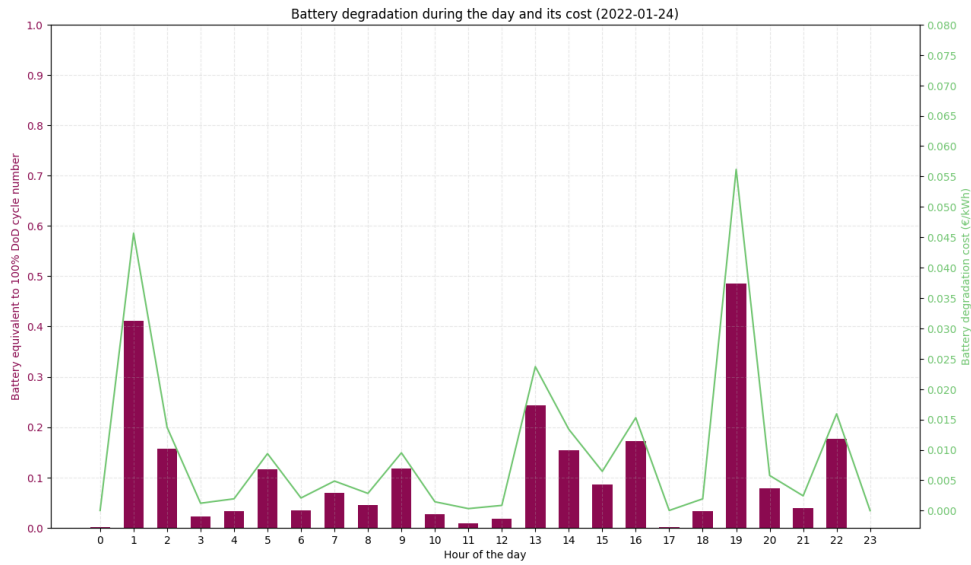
Figure 4.12: Second-life battery's degradation during 2022-01-24 and its cost
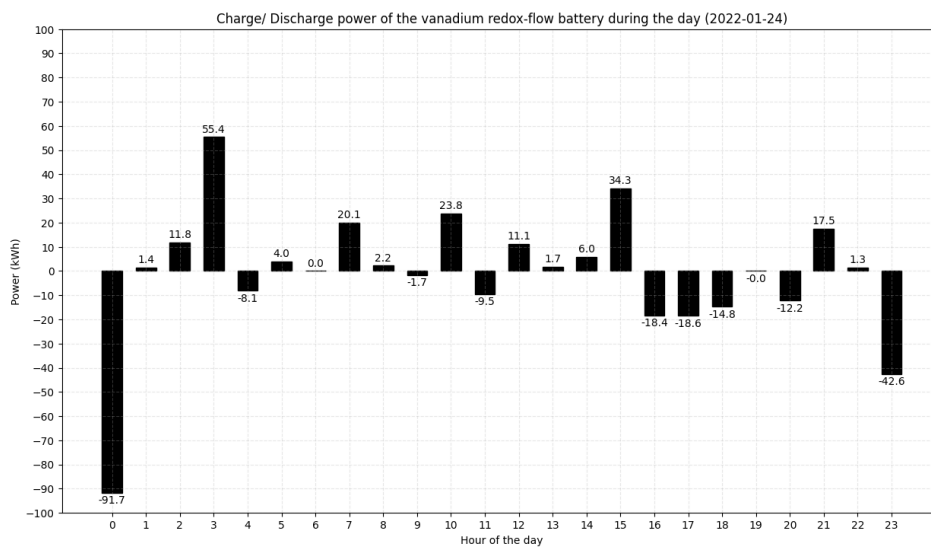
Figure 4.13: Charge/Discharge power of the vanadium redox-flow battery during 2022-01-24

But then, what can lead to these different charging and discharging behaviors between batteries? Well, these differences are mainly related to their specific properties and applications. It is important to note that these patterns can be influenced by factors such as the storage capacity, internal chemistry, life cycle and overall health status of the batteries.
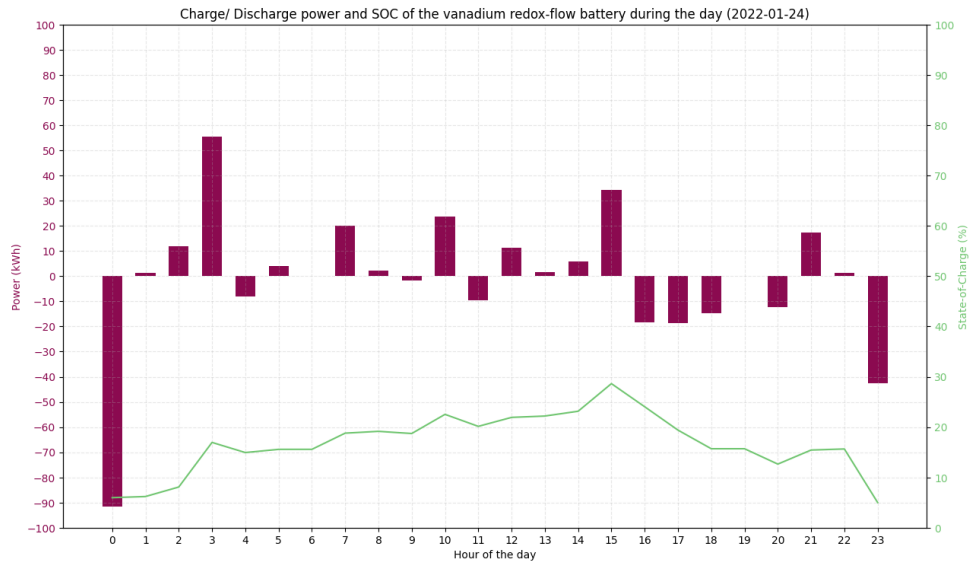
Figure 4.14: Charge/Discharge power of the vanadium redox-flow battery and its SOC during 2022-01-24

Optimizing for a random day provides valuable insights into the interaction between the different components of the system. By analyzing the performance of these elements in a short time frame, we can identify weaknesses, points of improvement and opportunities for enhancement to achieve a more efficient and sustainable operation.

The values corresponding to the optimization for this day are summarized in table 4.5.

Table 4.5: Results for battery charge and discharge during 2022-01-24

Description	Value
total energy charged in the second-life battery	754.30 [kWh]
total energy discharged in the second-life battery	611.09 [kWh]
total energy charged in the vanadium redox-flow battery	190.62 [kWh]
total energy discharged in the vanadium redox-flow battery	217.56 [kWh]
power imported from the grid	16494.56 [kW]
power exported to the grid	0 [kW]

Performing the calculations for the objective functions outlined in Section 3.2.1, enables to determine specific operation prices for 24 of January of 2022.

Costs related to system operation are in the order of 3752.41 €. The daily cost of second life battery degradation is around 0.24 €. Finally, the costs associated with carbon emissions are approximately 522.68 €. Costs associated with battery degradation are low compared to the others. Also, prices associated with system operation are, as expected, the highest.

4.3.3 Scenario 2: Optimization for a whole month in 2022

After the detailed optimization for a random day, the analysis was extended to a broader period, addressing the challenge of optimizing the operation for an entire month. In this case, the month chosen was August 2022. This lengthening of the study period will make it possible to identify relevant seasonal trends and patterns.

It is important to note that after running the optimisation for the whole month, some days with non-feasible solutions were identified. However, in order to simplify the analysis, it was filtered to select only the days with feasible solutions, which allows for the construction of a scenario with favourable and technically feasible conditions for the operation of the project, providing a more precise and targeted view of the results. That said, days 8,9,11,12,13,15,17,27,28,29,30 and 31 were excluded. Later, this issue will be re-addressed.

Similar to what was done for scenario 1, a detailed analysis of the charge and discharge cycle of two different batteries over the month of August was done. The aim was to understand the performance and behavior of these batteries in relation to their energy storage and release capacity. To gain valuable insights, the charge and discharge data of both batteries were recorded on a daily basis, tracking their variations over the study period.

Initially it was thought to make a representation of the SOC of both batteries over the 456 hours per month (the sum of the daily hours of the 19 feasible days studied), as shown in figure 4.15. However, it was only necessary to look at it to realize that this was not the best form of representation and that it would be extremely difficult to draw any conclusions about the data.
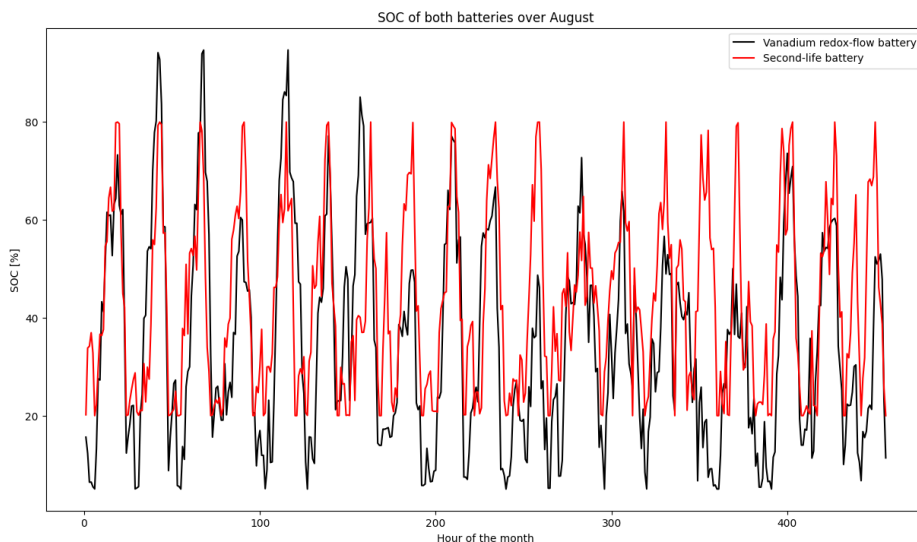

Figure 4.15: SOC of both batteries over August

Thus, it was decided to model a boxplot graphic. These graphics represent the distribution of data and their summary statistics, allowing to visualize the dispersion, asymmetry and possible

outliers in a set of values. the place where the vertical rod starts (from bottom to top) indicates the minimum (except for some possible extreme value or outlier) and where the rod ends indicates the maximum of the set. The rectangle in the middle of this rod has 3 lines: the top, the bottom and the inner line. The top line indicates the first quartile, i.e. the position of the first 25% of the data; the bottom line indicates the third quartile; and the inner line represents the median (a measure of position representing the midpoint of the distribution). The points that sometimes appear in the boxplot indicate that those observations are atypical, the so-called outliers.

The x-axis of the box plot represents the hours of the day, from 0 to 23. The y-axis represents the battery charge and discharge values. For each hour of the day, a data set containing all the charge and discharge measurements for that specific hour is verified, considering the 31 days of the month of August. The graphic, now presented in 4.16 concern the SOC of the second-life battery over the month. Analysing the figure, it is possible to see that the highest median is at 6 PM and the lowest at 12AM/12 PM.
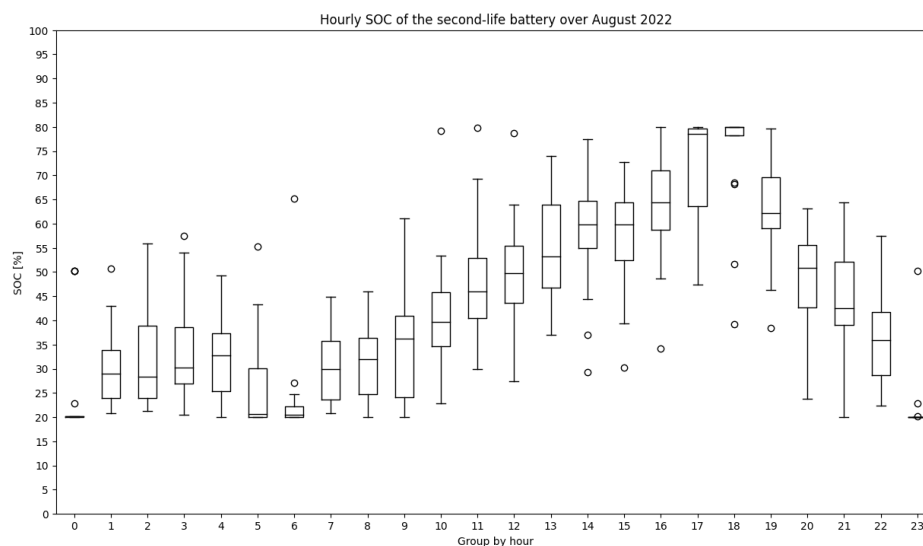
Figure 4.16: SOC of the second-life battery over August

The same procedure was also carried out for the vanadium redox-flow battery, and the results are shown in the graphic 4.17. A quick reading of this graphic reveals that the highest median is at 5pm and the lowest at 11pm.

By examining the figures 4.16 and 4.17 it is possible to spot some similarities between them, especially the tendency for them to discharge mostly at the end of the day, reaching SOC values very close to the respective minimum limits imposed by each battery.

For the analysis of the charging and discharging behavior of the batteries, illustrated in 4.18 and 4.19, it was decided to also model a boxplot graphic, representing on the x-axis again all the hours of the day for the month of August and on the y-axis the corresponding charge/ discharge
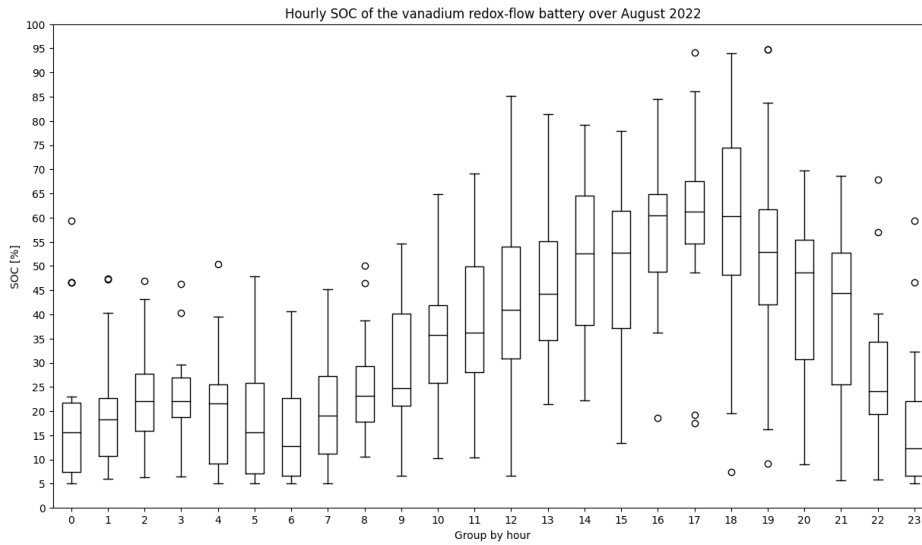
Figure 4.17: SOC of the vanadium redox-flow battery over August

values (in kW). As mentioned above, the 4.18 and 4.19 graphics were modeled, corresponding to the charge and discharge values of the second-life and vanadium redox-flow batteries, respectively, throughout August.
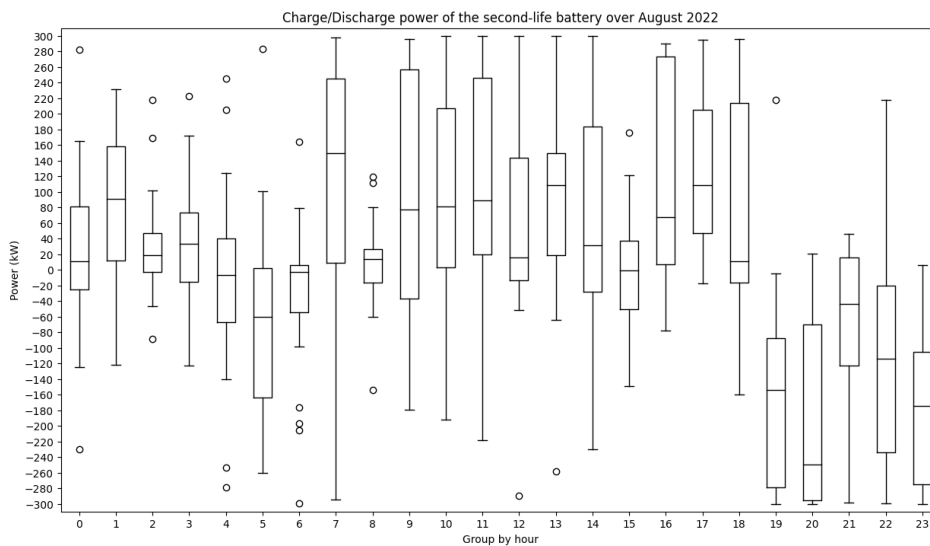
Figure 4.18: Charge/Discharge power of the second-life battery over August

From what is presented in 4.18, most hours are marked with outliners due to extreme variations in battery charge/discharge. The lowest median is reached at 9 PM and the highest at 7 AM. The
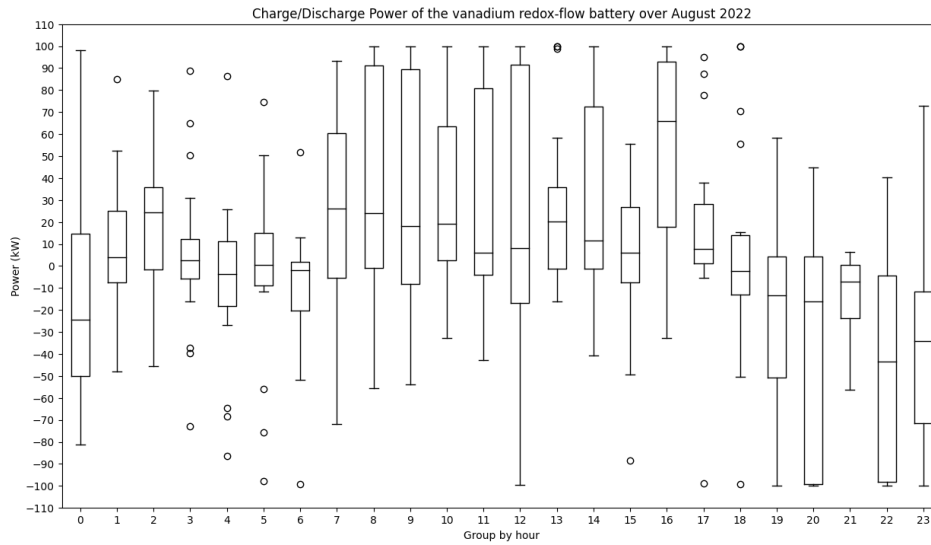
Figure 4.19: Charge/Discharge power of the vanadium redox-flow battery over August

hour with the highest dispersion, i.e. in which the data show the highest variability, is at 9 AM, and the hour with the lowest dispersion (i.e. lowest variability of results) corresponds to 8 AM.

Similarly, numerous outliners are also shown in 4.19, with the hour with the highest dispersion at 12 PM, and the hour with the lowest dispersion at 3 AM.In addition, the lowest median is reached at 8 PM, and the highest at 4 PM.

In addition, it should be mentioned that the state of charge of the vanadium redox-flow and the second-life battery (and obviously their charging/discharging as well) show similar changes over time, suggesting a parallel upward and downward trend. This similarity in SOC variations is an indication that these batteries can be very complementary and efficient when working together. This compatibility makes the use of these batteries together a promising choice in energy storage systems and other applications where stable energy output is essential.

Battery charge and discharge information for the month of August is summarized in table 4.6.

Table 4.6: Results for battery charge and discharge over August

Description	Value
total energy charged in the second-life battery	28878.45 [kWh]
total energy discharged in the second-life battery	23998.16 [kWh]
total energy charged in the vanadium redox-flow battery	9880.01 [kWh]
total energy discharged in the vanadium redox-flow battery	6882.70 [kWh]
power imported from the grid	163366.84 [kW]
power exported to the grid	562188.47 [kW]

It can be seen that the second-life battery charged and discharged more than the vanadium

redox-flow battery. This information indicates that the second-life battery may have been used more and subjected to more cycles, which may have an impact on its life and performance.

Again, these values are substituted into the target functions. The costs associated with carbon emissions are around 5167.63€; the costs associated with the monthly degradation of the second life battery are, again, not very significant, and are around 9.47€. Beyond this, the costs on importing energy from the grid are in the range of 23824.43€, and 11243.77€the profit on exporting energy to the grid, which results in an total cost of operating the system around 12580.66€.

4.3.4   Scenario 3: Optimization for the entire year 2022

After performing the optimization for 1 day, and then for 1 month, let's now focus on taking a broader view of the problem: 1 whole year. Similarly to what happened in the previous scenario, we ran into the same issue of there being days with non-feasible solutions, so these were excluded from the analysis.

That said, this scenario aims to do just that, translating into the appearance of more complex challenges that require a more strategic and sustainable approach - now it can't just take immediate efficiency into account, but continuous and consistent success in a long-term scenario.

Taking a long-term view of the project is undoubtedly an essential part of strategic vision in any field. Given that one of the main objectives of this problem is to minimize costs (i.e. maximize profits), optimizing at 1 year can lead to a higher profit margin over time, as efficient operations result in less waste and greater productivity.

As in previous scenarios, let's start by analyzing the charge and discharge cycles of both batteries throughout 2022. This creates the possibility to identify usage patterns, degradation trends and potential opportunities for improvement. This analysis is the foundation on which we will build effective optimization strategies to ensure that batteries meet our needs reliably and efficiently over the next year.

Once again, as before, boxplot graphics were chosen to display the data: the hours from 0 to 23 are on the x-axis, representing a comprehensive analysis of the battery's behavior over the course of a full year, divided into one-hour intervals. Each point on the x-axis represents an hour of the day, and the boxplot provides a statistical overview of the measurements or data collected at that specific time. Analogous to the previous scenarios, let's start by discussing the SOC of the second-life and vanadium redox-flow batteries, which are displayed graphically in figures 4.20 and 4.21, respectively.

As in scenario 2, batteries also tend to start the day with the SOC close to the minimum possible limit, increasing until a certain point in the day and then decreasing until they reach values close to the minimum again at the end of the day. In the case of the second-life battery, this point is at 5 PM, and in vanadium-redox flow batteries between 5 PM and 6 PM. This is indicative of similar behaviour, which shows that the batteries can be operated successfully together.

Next, boxplots were made of the charge and discharge power of both batteries throughout the year, on an hourly basis. These can be found at 4.23 and 4.22, and refer to the charge and discharge power of the second-life and vanadium redox-flow batteries, respectively.
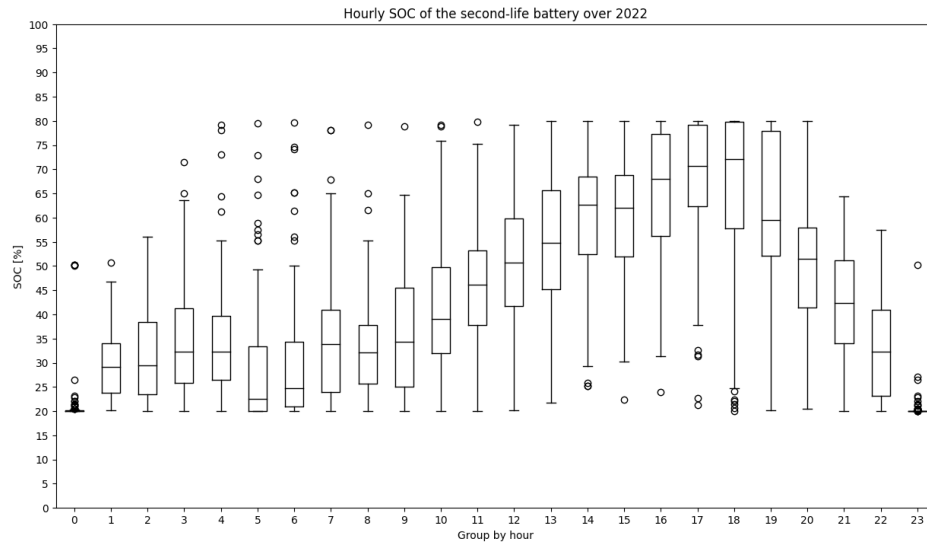
Figure 4.20: Hourly SOC of the second-life battery over 2022
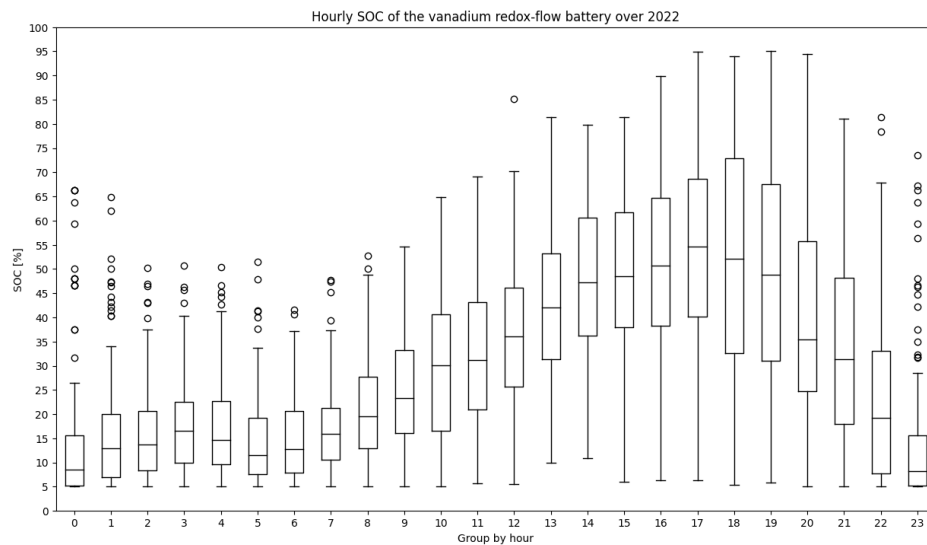
Figure 4.21: Hourly SOC of the vanadium redox-flow battery over 2022

From the outset, a battery with higher charge/discharge efficiencies will, in principle, be used more, as it leads to less energy loss and therefore lower costs (the main goal of all optimization). Graphically speaking, the battery with the greatest efficiency be the one that shows the least drop in power during the charge/discharge process. That said, and analysing 4.22 and 4.23, it turns out that this is the vanadium one.
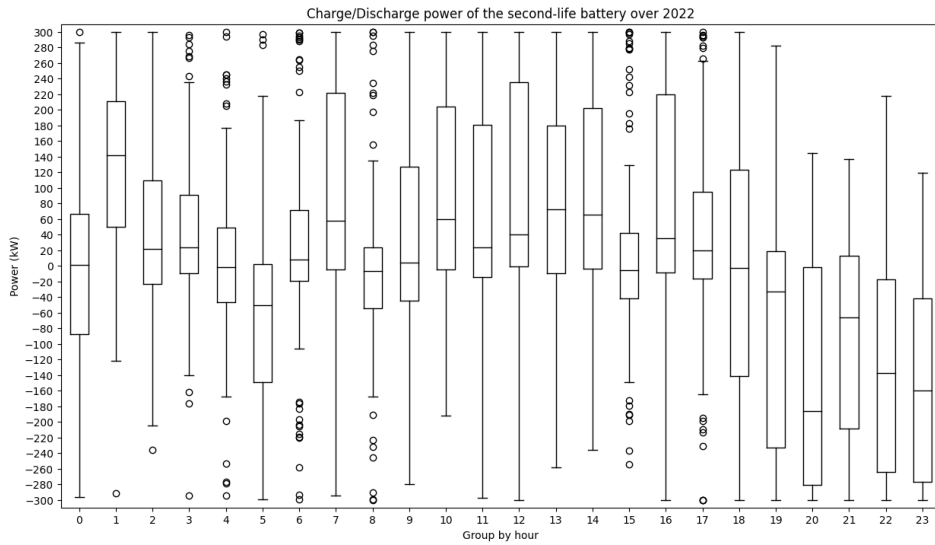
Figure 4.22: Charge/Discharge power of the second-life battery during 2022
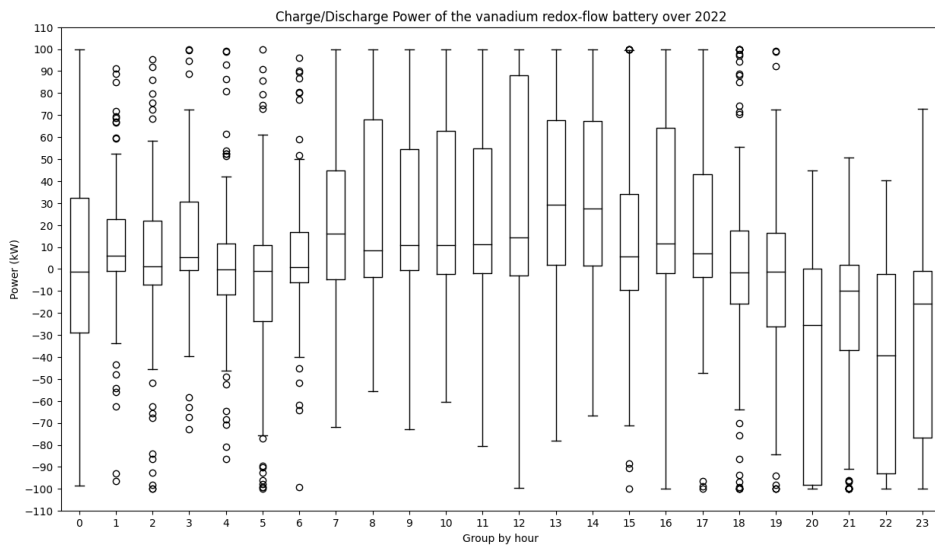
Figure 4.23: Charge/Discharge power of the vanadium redox-flow battery during 2022

Beyond this, a comparison was made between the energy consumed by the supercomputer and the PV energy generated now shown in figure 4.24. It can be seen that the consumption profile of the HPC system is relatively constant, while obviously PV generation tends to be higher in the summer months. Despite this, PV generation is never enough to meet the energy demand of a supercomputer. As a result, there is a need to import energy from the conventional electric-

ity grid to supplement solar production and ensure the continuous and efficient operation of the supercomputer. This combination of energy sources is a common strategy for balancing energy sustainability with the uninterrupted operation of critical systems, ensuring that the supercomputer is always available for its essential computing tasks.
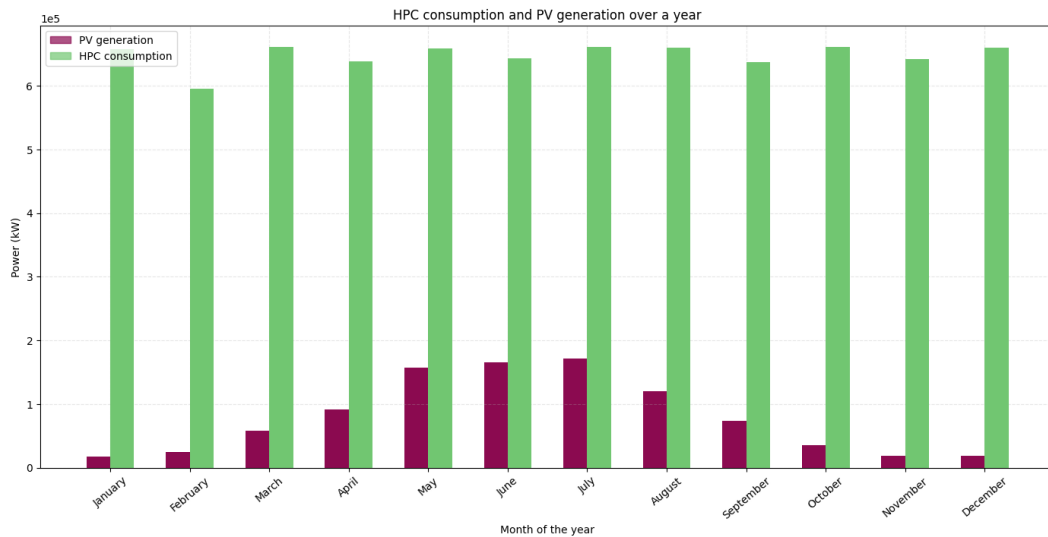
Figure 4.24: HPC consumption and PV generation over 2022

Finally, table 4.7 summarises the energy behaviour of batteries throughout 2022.

Table 4.7: Results for battery charge and discharge over 2022

Description	Value
total energy charged in the second-life battery	177291.56 [kWh]
total energy discharged in the second-life battery	146425.98 [kWh]
total energy charged in the vanadium redox-flow battery	57294.92 [kWh]
total energy discharged in the vanadium redox-flow battery	1179843.32 [kWh]
power imported from the grid	3117115.21[kW]
power exported to the grid	2973011.94 [kW]

Again, these values were substituted into the objective functions. The costs associated with carbon emissions are around 28574.71€; the costs associated with the monthly degradation of the second life battery are, again, not very significant, and are around 58.65€. The costs on importing energy from the grid round 196747.04€and the profit from exporting energy to the grid are about 59460.24€, resulting in a total system operating cost of about 137286.81€.

4.4 Economic analysis

In the global energy market, renewable energies are already well-established as reliable energy sources. The rapid expansion of renewable technologies has been largely attributed to their rising cost-effectiveness, ongoing financing, ongoing incentive programs and the rising need for energy on a worldwide scale. That said, the implementation of solar photovoltaic (PV) power generation projects has become increasingly common due to their environmental and financial benefits, as well as possible ways of storing this energy.

In order to assess the viability and success of projects, three key metrics stand out: the Levalized Cost of Electricity (LCOE), the Levalized Cost of Storage (LCOS), and the Payback Period.

4.4.1 LCOE

LCOE refers to the average cost (in €) per MWh of energy produced by the system [51]. This indicator accounts for the initial investment, maintenance costs throughout the project's useful life, and the overall amount of electricity produced. It is computed by dividing all costs generated by the energy system, by the amount of energy produced by that same system. The formula which illustrates this can be consulted in 4.1.

$$LCOE = \frac{\sum_{n=0}^{N} \left(\frac{Inv_n + O\&M_n}{(1+r)^n} \right)}{\sum_{n=0}^{N} \left(\frac{E_n}{(1+r)^n} \right)} \tag{4.1}$$

where n represents the lifetime of the project, $O\&M_n$ refers to the operation and maintenance costs in year n, r to the discount rate , Inv_n to the investment in the project, and E_n to the amount of electricity in each year, in MWh. Table 4.8 summarizes all this input information required to calculate LCOE.

Table 4.8: Inputs required for LCOE calculation

Description	Parameter	Unit	Value
Period Analysis	N	years	20
year n	n		
PV energy generation	E_n	MWh/year	952.48631
PV capacity	$PV_{capacity}$	MW	1
PV System Cost	Inv_n	€/kW	1340
PV O&M Costs	$O\&M_n$	€/kW	20.1
Discount Rate	r	%	10

As stated in subsection 4.2.3, data regarding PV generation throughout the year were produced synthetically using the Python PVlib library, via PVGIS (Photovoltaic Geographical Information System), and in the graphic in 4.6 shows the results obtained, in the form of a monthly sum of PV generation over 2022. Adding up all these values, it is possible to then obtain the annual PV energy

production: 952486.31 kWh i.e. 952.48631 MWh. At the time of implementing that function, the capacity of the PV system was established to be 1 MWp.

Regarding the costs over the life of the system, the investment in it should be emphasised, as well as the costs associated with operating and maintaining it. Based on [52], it was established that the photovoltaic panel systems cost is approximately 1340€ per kWp. Maintenance and operating costs were assumed to be around 1.5% of the total cost of the system [53].

The project's lifetime (*n*) is 20 years, and a discount rate (*r*) of 10% is considered.

To calculate the LCOE, it is essential to have the Net Present Value (NPV) associated with the project. The NPV takes into account the cash-flows over time, considering costs, investments and the discount rate. It plays a key role in economic evaluation, and in determining the LCOE. Below, table 4.9 shows the net NPV values, detailing the various elements that make up this essential financial analysis.

Table 4.9: Calculation of cash-flow's NPV

	Input Data		NPV		Periods																			
				0	1	2	3	4	5	6	7	8	9	10	11	12	13	14	15	16	17	18	19	20
PV Generation	[MWh/ year]	952.48631	19 049.7262	-	952.48631	952.48631	952.48631	952.48631	952.48631	952.48631	952.48631	952.48631	952.48631	952.48631	952.48631	952.48631	952.48631	952.48631	952.48631	952.48631	952.48631	952.48631	952.48631	952.48631
PV Cost	[€]	1340000	1 340 000	1340000	-	-	-	-	-	-	-	-	-	-	-	-	-	-	-	-	-	-	-	-
O&M Cost	[€]	20100	171 122.63	-	20100	20100	20100	20100	20100	20100	20100	20100	20100	20100	20100	20100	20100	20100	20100	20100	20100	20100	20100

PV cost is obtained by multiplying the value of Inv_n (PV system cost per €/kW) by the total kWp of the system (which in this case is 1,000), giving a total investment of 1 340 000€ in equipment in year 0. That equipment is expected to operate reliably and efficiently over a 20 year period, without the need for replacement.

In order to calculate PV generation over the project's lifetime, it is assumed that there is no generation at all in year 0, taking only values from year 1 to year 20. Those values are kept constant over the 20 years, as no major variations are expected from year to year, given the stability of conditions on site. The sum of all these values gives a total PV energy production of 19 049.7262 MWh.

Finally, with regard to the costs associated with operating and maintaining the system, and considering that these are 1.5% of the system's total costs, as mentioned before, this gives an annual amount of 20 100€ (0.015 * 1 340 000). Once again, considering that these only exist from year 1 to year 20, the NPV associated with the parameter was subsequently calculated, considering a discount rate of 10%, which culminates in a total cost of 171 122.63€.

Now that all the parameters have an assigned value, substituting them in their respective places in the formula 4.1 gives an LCOE corresponding to 79.33 €/MWh. This means that the average cost of producing 1 MWh of electricity from the PV source in question is €79.33 over the lifetime of the project, which turns out to be a relatively normal value for this parameter, according to, for example, the work carried out in [54].

4.4.2 LCOS

LCOS - Levalised Cost of Storage - is a metric that allows a quick assessment of the economic viability of a storage technology in a specific electricity market [55]. One of its biggest limitations

is that it doesn't reflect possible income earned by the storage owner from servicing ancillary services (such as energy sales).

It is calculated according to the equation (from the work of [55]) below:

$$LCOS = \frac{\sum_{n=0}^{N} (Capital_n + O\&M_n + Fuel_n) \cdot (1+r)^{-n}}{\sum_{n=0}^{N} (MWh_n) \cdot (1+r)^{-n}} \tag{4.2}$$

where $Capital_n$ refers to the capital expenditures in year n, $O\&M_n$ concerns the operation and maintenance costs of the equipment in year n, $Fuel_n$ represents the charging costs in year n and, finally, MWh_n relates to the amount of electricity discharged in MWh in year n.

Within the scope of this analysis, the two distinct energy storage technologies discussed throughout the dissertation have been studied carefully. Each of these technologies will be discussed in detail separately, allowing their individual characteristics, advantages and challenges to be addressed. This segmented approach provides a deeper understanding of how these technologies operate independently. However, the analysis is not limited to these isolated considerations. Later, the scenario of the two technologies interacting in a joint operation will be explored.

Starting with the second-life battery, the specific characteristics of this type of battery are described in detail in the table 4.10.

Table 4.10: Inputs required for LCOS calculation for the second-life battery

Description	Parameter	Unit	Value
Period Analysis	N	years	20
year n	n		
Discount Rate	r	%	10
Battery Capacity	$b_{capacity}$	kW	1500
Battery Cost	b_{cost}	€/kWh	117
O&M Cost	$O\&M_{cost}$	€/kW/year	1.755
Durability of a battery	b_{years}	years	12
Nº of batteries used in the project	b_{number}	-	2

The table shows that, as expected, the period of analysis remains at 20 years, as does the discount rate, which remains 10%.

The battery capacity is 1500 kW, a value that was previously mentioned when the battery data was presented at the beginning of this chapter. It is also assumed that the battery has a lifespan of 12 years, so for the project in question, 2 batteries will be needed (so that there can be a replacement in year 12). The cost of the battery comes to 117 €/kWh, according to [56], and again, the cost of operation and maintenance is assumed to be 1.5% of this value, resulting in 1.755 €/kWh/year.

Taking battery capacity into account, the total purchase cost of each battery is calculated as 1500 €/kWh * 1500 kW, which is 175 500 €. With the percentage calculation associated with the O&M costs, the annual costs of this magnitude are in the order of 2632.5 €.

In addition, it is also necessary to determine the values of $Fuel_n$ and MWh_n in order to effectively calculate the LCOS.

When modelling the battery, a piece of code was developed to be responsible for adding up all the charge values of the device, as well as another to do the same, but with all the discharge values of it (taking into account only the days of the year with feasible solutions). As a result of this, it is known that the power charged by the battery during the year 2022 was 177 291.5576 kWh, and the power discharged by it was 146 425.9779 kWh.

As already mentioned, the value of MWh_n refers to the discharge of the second-life battery over 20 years (assuming that this power is always the same throughout the project, once again, because no major variations are expected in terms of system operation), which results in 292 851.558 kWh, and, this value must be presented in MWh, thus obtaining a MWh_n of 2 928.519558 MWh.

The value of $Fuel_n$, as known, represents the charging costs in year n. To calculate this parameter two things need to be known: the power charged annually by the battery (which was already recognised), and the cost associated with charging it. Since all the energy load supplied to the system comes exclusively from the PV system, the costs associated with this were assumed as the value being given by the value of the LCOE (which is also known). So, on an annual basis, which results in a final figure of 14 063.68€ per year.

As was the case when calculating the LCOE, the NPV of each monetary item was then calculated. These calculations are summarised in 4.11.

Table 4.11: NPV's calculation for the second-life battery monetary costs

INPUT DATA			PERIODS																				NPV
Parameter	Unit	Value per year	0	1	2	3	4	5	6	7	8	9	10	11	12	13	14	15	16	17	18	20	
Battery Cost	€/year	175 500	175 500	-	-	-	-	-	-	-	-	-	-	-	175 500	-	-	-	-	-	-	-	231 419.71 €
O&M Cost	€/year	2 632.5	-	2 632.5	2 632.5	2 632.5	2 632.5	2 632.5	2 632.5	2 632.5	2 632.5	2 632.5	2 632.5	2 632.5	2 632.5	2 632.5	2 632.5	2 632.5	2 632.5	2 632.5	2 632.5	22 411.96 €
Fuel	€/MWh	14 063.68	-	14 063.68	14 063.68	14 063.68	14 063.68	14 063.68	14 063.68	14 063.68	14 063.68	14 063.68	14 063.68	14 063.68	14 063.68	14 063.68	14 063.68	14 063.68	14 063.68	14 063.68	14 063.68	119 732.05 €

After completing these steps, all the necessary parameters for calculating the LCOS are gathered. Table 4.12 gives an outline of them.

Table 4.12: Final parameters to LCOS' calculation on second-life battery

Parameter	Value	Unit
N	20	[years]
r	10	[%]
$Capital$	231 419.71	[€]
$O\&M$	22 411.96	[€]
$Fuel$	119 732.05	[€]
MWh	2 928.519558	[MWh]

Plugging these values into the equation 4.2 results a LCOS value of 127.56 €/MW.

This whole process was then repeated, but this time for the vanadium redox-flow battery. The characteristics of this battery appear below in table 4.13.

Compared to the previous case, the only differences lie in the battery cost, which here is assumed to be 300 €/kW (according to the work of [57]), and the battery capacity, which is 500

Table 4.13: Inputs required for LCOS calculation for the vanadium redox-flow battery

Description	Parameter	Unit	Value
Period Analysis	N	years	20
year n	n		
Discount Rate	r	%	10
Battery Capacity	$b_{capacity}$	kW	500
Battery Cost	b_{cost}	€/kWh	300
O&M Cost	$O\&M_{cost}$	€/kW/year	4.5
Durability of a battery	b_{years}	years	12
Nº of batteries used in the project	b_{number}	-	2

kW, as already known from the beginning of the chapter. As a result, the total cost of the battery is 150 000 €, and the operating and maintenance costs are 2 250 €.

Through the use of methods similar to those presented in the above scenario, the battery's total annual charge and discharge values in 2022 were also calculated, which are 57 294.92315 kWh and 37 603.8396 kWh, respectively.

As a result, the value of MWh_n is 752,076792 MWh (from the sum of the 37,603,8396 kW discharged annually over 20 years).

The annual value of $Fuel_n$ was further calculated by multiplying the power charged annually through the battery by the respective LCOE value, resulting in 4 544.93 €.

The NPV of each currency was calculated as well, and their respective values are listed in table 4.14.

Table 4.14: NPV's calculation for the second-life battery monetary costs

Parameter	Unit	Value per year	0	1	2	3	4	5	6	7	8	9	10	11	12	13	14	15	16	17	18	20	NPV
Battery Cost	€/year	150000	150000	-	-	-	-	-	-	-	-	-	-	-	150000	-	-	-	-	-	-	-	197 794.62 €
O&M Cost	€/year	2 250	-	2 250	2 250	2 250	2 250	2 250	2 250	2 250	2 250	2 250	2 250	2 250	2 250	2 250	2 250	2 250	2 250	2 250	2 250	2 250	19 155.52 €
Fuel	€/MWh	4 544.93	-	4 544.93	4 544.93	4 544.93	4 544.93	4 544.93	4 544.93	4 544.93	4 544.93	4 544.93	4 544.93	4 544.93	4 544.93	4 544.93	4 544.93	4 544.93	4 544.93	4 544.93	4 544.93	4 544.93	38 693.54 €

After having done this, all the values needed to calculate the LCOS are gathered together. Table 4.15 gives a final overview of them.

Table 4.15: Final parameters to LCOS' calculation on vanadium redox-flow battery

Parameter	Value	Unit
N	20	[years]
r	10	[%]
$Capital$	197 794.62	[€]
$O\&M$	19 155.52	[€]
$Fuel$	38 693.54	[€]
MWh	752.076792	[MWh]

Replacing the values of 4.15 in equation 4.2, results in a LCOS of 339.92 €/MWh.

To conclude, a scenario was computed in which the two batteries operate together. To calculate the LCOS in this case, it is only necessary to combine the parameters for each of the previous batteries in the same equation. The combined value of each parameter is presented in table 4.16.

Table 4.16: Final parameters to LCOS' calculation on both batteries working together

Parameter	Value	Unit
N	20	[years]
r	10	[%]
Capital	429 214.33	[€]
O&M	41 567.47	[€]
Fuel	158 425.59	[€]
MWh	3 680.59635	[MWh]

This leads to an LCOS value for the whole operation of €170.95/MWh.

So now that the three different scenarios have been analysed, let's compare them. The LCOS calculation values for each technology are summarised in table 4.17.

Table 4.17: LCOS' values for the different technologies studied

Technology	LCOS
Second-life battery	127.56 €/MWh
Vanadium redox-flow battery	339.92 €/MWh
Second life + Vanadium redox-flow batteries	170.95 €/MWh

Second-life battery technology shows the lowest cost, and vanadium redox-flow battery the highest, which is proof that reused EV batteries are, as expected, more economical solutions in terms of energy storage than completely new batteries. The combination of technologies has an LCOS of 170.95 €/MWh, which indicates that this hybrid approach can provide a balance between cost and performance.

This suggests that using second-life batteries in conjunction with vanadium flow batteries could be an effective strategy for optimizing the cost of energy storage.

Chapter 5

Conclusions and Future Work

These conclusions and future work chapter represents a crucial moment to reflect on the significant findings that have shaped our understanding. Moreover, it offers a prospective view of potential directions that can be pursued, paving the way for further opportunities for improvement in this work.

Overall, the knowledge gained from the optimization scenarios' outcomes was helpful in understanding how a data center would operate and behave with the addition of second-hand batteries and vanadium redox-flow batteries. The analysis of the Li-ion battery's transition from first to second life showed the viability of recycling old electric vehicle batteries by demonstrating that there are still a significant number of cycles left in the second life. The possibility of these batteries having a second life is further supported by the low degradation per full charge/discharge cycle, which can help the improvement of the sustainability of energy storage solutions. The optimization approach considered not only the economic aspects but also the environmental impact, making it possible to design a system that balances the commitments between costs and energy storage performance.

The study provided insight into the interactions between the various parts of the system and made it possible to pinpoint crucial times for battery operation in the optimization for a random day in 2022. When compared to the second-life battery, which serves as supplemental power, the vanadium redox-flow battery showed more abrupt charging and discharging characteristics. The second-life battery's cost of degradation was demonstrated to be directly connected with its operation, highlighting the significance of optimizing the battery's performance to reduce costs and increase lifespan.

Extending the analysis to the optimization for an entire month in August 2022 it was realized that the SOC variations of both batteries demonstrated the typical charging and discharging cycles observed in daily operation, with higher SOC values at the beginning of the day and lower SOC values by the end. The charge and discharge behaviors for both batteries varied throughout the day, with certain periods exhibiting extreme variations and others showing more stability.

Finally, carrying out the analysis for the whole of 2022, annual optimization proved to be a fundamental process for maximizing efficiency and performance over time.

By considering long-term and short-term optimization scenarios, this research laid the foundation for sustainable energy storage solutions that can enhance the efficiency of data center operations.

In the following subsection some proposals for future works are presented in order to improve the obtained results.

5.1   Future Work

Technological innovation in the area of data center energy management is a promising field, but its practical implementation encounter a lot of challenges that need to be addressed. It is important to recognize that, like all research, it has limitations inherent to the approach adopted.

It stands out that there are non-feasible days when running the optimization, both for the monthly and annual context. These "non-feasible days" refer to situations in which the algorithm was unable to find optimal or effective solutions due to complexities, restrictions or problems inherent in the system under analysis. This may be due to limitations in the algorithm, such as its ability to cope with the complexity of the data or constraints set. It may also reflect the need to improve the modeling of the data and constraints underlying the optimization problem. In addition, a lack of convergence or sub-optimal solutions may indicate that the algorithm is not exploring the solution space effectively. That said, it is essential to improve the optimization algorithm in order to, in the future, obtain better results.

Regardless these limitations, the insights gained through this research open new horizons and lay a solid foundation for future investigations.

One of the main directions for future work involves exploring new approaches to limit the lifetime of batteries, with the aim of minimizing their degradation over time. Instead of just optimizing the objective function to find the optimal maintenance point, one could incorporate a constraint that specifies the desired duration for battery life. For example, instead of minimizing maintenance costs over a planning horizon, one could explicitly state how long one wants the equipment to last under certain operating conditions. In addition, another promising approach is to implement constraints that limit the number of daily operating cycles of the equipment so that it can last as long as desired. These new ways of limiting equipment lifetime may provide more realistic and feasible solutions, ensuring more balanced wear over time and reducing degradation.

Another promising future work is the consideration and development of more complex models to represent the battery behavior in a more accurate and comprehensive way, especially for the vanadium redox-flow battery, which in this dissertation was represented by the bucket model, one of the most simplistic battery representation models.

In the future other renewable energy sources than the one considered in this dissertation (e.g. wind) can also be exploited, making the whole operation even more sustainable.

Finally, and in addition to what has already been mentioned above, the optimization can be further improved by entering the thermal part of the system, optimizing the cooling at different times of the day, as well as the scheduling of the computational processes of the supercomputer,

in order to obtain a controllable load that allows aligning the electrical consumption with the most favorable hours to consume energy.

References

[1] C. Sarkar, "Data center network design," 05 2010.

[2] G. Mehta, G. Mittra, and V. K. Yadav, "Application of iot to optimize data center operations," in *2018 International Conference on Computing, Power and Communication Technologies (GUCON)*, pp. 738–742, 2018.

[3] T. Hoefler, A. Hendel, and D. Roweth, "The convergence of hyperscale data center and high-performance computing networks," *Computer*, vol. 55, no. 7, pp. 29–37, 2022.

[4] W.-c. Feng, X. Feng, and R. Ge, "Green supercomputing comes of age," *IT Professional*, vol. 10, no. 1, pp. 17–23, 2008.

[5] Z. Cao, X. Zhou, H. Hu, Z. Wang, and Y. Wen, "Toward a systematic survey for carbon neutral data centers," *IEEE Communications Surveys Tutorials*, vol. 24, no. 2, pp. 895–936, 2022.

[6] A. Radovanovic, R. Koningstein, I. Schneider, B. Chen, A. Duarte, B. Roy, D. Xiao, M. Haridasan, P. Hung, N. Care, S. Talukdar, E. Mullen, K. Smith, M. Cottman, and W. Cirne, "Carbon-aware computing for datacenters," 2021.

[7] O. Marra, M. Mirto, and M. Cafaro, "Green computing and power saving in hpc data centers," *SSRN Electronic Journal*, 12 2011.

[8] J. Guitart, "Toward sustainable data centers: a comprehensive energy management strategy," *Computing*, vol. 99, 06 2017.

[9] V. D. Reddy, B. Setz, G. S. V. R. K. Rao, G. R. Gangadharan, and M. Aiello, "Metrics for sustainable data centers," *IEEE Transactions on Sustainable Computing*, vol. 2, no. 3, pp. 290–303, 2017.

[10] W. Khan, D. De Chiara, A.-L. Kor, and M. Chinnici, "Exploratory data analysis for data center energy management," in *Proceedings of the Thirteenth ACM International Conference on Future Energy Systems*, e-Energy '22, (New York, NY, USA), p. 571–580, Association for Computing Machinery, 2022.

[11] C. Peoples, G. Parr, and S. McClean, "Energy-aware data centre management," in *2011 National Conference on Communications (NCC)*, pp. 1–5, IEEE.

[12] H. Rong, H. Zhang, S. Xiao, C. Li, and C. Hu, "Optimizing energy consumption for data centers," *Renewable and Sustainable Energy Reviews*, vol. 58, pp. 674–691, 2016.

[13] K. A. Horowitz, Z. Peterson, M. H. Coddington, F. Ding, B. O. Sigrin, D. Saleem, S. E. Baldwin, B. Lydic, S. C. Stanfield, N. Enbar, S. Coley, A. Sundararajan, and C. Schroeder,

"An overview of distributed energy resource (der) interconnection: Current practices and emerging solutions,"

[14] J. M. Reniers, G. Mulder, S. Ober-Blöbaum, and D. A. Howey, "Improving optimal control of grid-connected lithium-ion batteries through more accurate battery and degradation modelling," *Journal of Power Sources*, vol. 379, pp. 91–102, 2018.

[15] H. Li, "Practical evaluation of li-ion batteries," *Joule*, vol. 3, no. 4, pp. 911–914, 2019.

[16] A. Manthiram, "An outlook on lithium ion battery technology," *ACS Central Science*, vol. 3, no. 10, pp. 1063–1069, 2017. PMID: 29104922.

[17] D. Deng, "Li-ion batteries: basics, progress, and challenges," *Energy Science & Engineering*, vol. 3, no. 5, pp. 385–418, 2015.

[18] M. Chen and G. Rincon-Mora, "Accurate electrical battery model capable of predicting runtime and i-v performance," *IEEE Transactions on Energy Conversion*, vol. 21, no. 2, pp. 504–511, 2006.

[19] M. Fanoro, M. Božanić, and S. Sinha, "A review of the impact of battery degradation on energy management systems with a special emphasis on electric vehicles," *Energies*, vol. 15, no. 16, 2022.

[20] X. Han, L. Lu, Y. Zheng, X. Feng, Z. Li, J. Li, and M. Ouyang, "A review on the key issues of the lithium ion battery degradation among the whole life cycle," *eTransportation*, vol. 1, p. 100005, 2019.

[21] R. Guo, L. Lu, M. Ouyang, and X. Feng, "Mechanism of the entire overdischarge process and overdischarge-induced internal short circuit in lithium-ion batteries," *Scientific reports*, vol. 6, no. 1, p. 30248, 2016.

[22] J. S. Edge, S. O'Kane, R. Prosser, N. D. Kirkaldy, A. N. Patel, A. Hales, A. Ghosh, W. Ai, J. Chen, J. Yang, S. Li, M.-C. Pang, L. Bravo Diaz, A. Tomaszewska, M. W. Marzook, K. N. Radhakrishnan, H. Wang, Y. Patel, B. Wu, and G. J. Offer, "Lithium ion battery degradation: what you need to know," *Phys. Chem. Chem. Phys.*, vol. 23, pp. 8200–8221, 2021.

[23] E. Martinez-Laserna, E. Sarasketa-Zabala, D.-I. Stroe, M. Swierczynski, A. Warnecke, J. Timmermans, S. Goutam, and P. Rodriguez, "Evaluation of lithium-ion battery second life performance and degradation," in *2016 IEEE Energy Conversion Congress and Exposition (ECCE)*, pp. 1–7, 2016.

[24] M. Shahjalal, P. K. Roy, T. Shams, A. Fly, J. I. Chowdhury, M. R. Ahmed, and K. Liu, "A review on second-life of li-ion batteries: prospects, challenges, and issues," *Energy*, vol. 241, p. 122881, 2022.

[25] E. Hossain, D. Murtaugh, J. Mody, H. M. R. Faruque, M. S. Haque Sunny, and N. Mohammad, "A comprehensive review on second-life batteries: Current state, manufacturing considerations, applications, impacts, barriers potential solutions, business strategies, and policies," *IEEE Access*, vol. 7, pp. 73215–73252, 2019.

[26] F. Salek, A. Azizi, S. Resalati, P. Henshall, and D. Morrey, "Mathematical modelling and simulation of second life battery pack with heterogeneous state of health," *Mathematics*, vol. 10, no. 20, 2022.

[27] P. Cicconi, D. Landi, A. Morbidoni, and M. Germani, "Feasibility analysis of second life applications for li-ion cells used in electric powertrain using environmental indicators," in *2012 IEEE International Energy Conference and Exhibition (ENERGYCON)*, pp. 985–990, 2012.

[28] C. L. Chen, H. K. Yeoh, and M. Chrakbarti, "An enhanced one-dimensional stationary model for the all-vanadium redox flow battery," 06 2013.

[29] A. Z. Weber, M. M. Mench, J. P. Meyers, P. N. Ross, J. T. Gostick, and Q. Liu, "Redox flow batteries: a review," vol. 41, no. 10, pp. 1137–1164.

[30] R. Chen, S. Kim, and Z. Chang, "Redox flow batteries: Fundamentals and applications," in *Redox* (M. A. A. Khalid, ed.), ch. 5, Rijeka: IntechOpen, 2017.

[31] G. Deiktas, A. G. Anastasiadis, and G. A. Vokas, "Economic investigation of a vanadium redox bess for the exploitation of wind power rejections in an isolated greek island," *Energy Reports*, vol. 6, pp. 367–379, 2020. Technologies and Materials for Renewable Energy, Environment and Sustainability.

[32] Y. R. Challapuram, G. M. Quintero, S. B. Bayne, A. S. Subburaj, and M. A. Harral, "Electrical equivalent model of vanadium redox flow battery," in *2019 IEEE Green Technologies Conference(GreenTech)*, pp. 1–4, 2019.

[33] M. Mohamed, H. Ahmad, M. A. Seman, S. Razali, and M. Najib, "Electrical circuit model of a vanadium redox flow battery using extended kalman filter," *Journal of Power Sources*, vol. 239, pp. 284–293, 2013.

[34] B. Xiong, Y. Yang, J. Tang, Y. Li, Z. Wei, Y. Su, and Q. Zhang, "An enhanced equivalent circuit model of vanadium redox flow battery energy storage systems considering thermal effects," *IEEE Access*, vol. 7, pp. 162297–162308, 2019.

[35] M. T. Islam and U. Iyer-Raniga, "Lithium-ion battery recycling in the circular economy: A review," *Recycling*, vol. 7, no. 3, 2022.

[36] E. Martinez-Laserna, I. Gandiaga, E. Sarasketa-Zabala, J. Badeda, D.-I. Stroe, M. Swierczynski, and A. Goikoetxea, "Battery second life: Hype, hope or reality? a critical review of the state of the art," *Renewable and Sustainable Energy Reviews*, vol. 93, pp. 701–718, 2018.

[37] H. Iqbal, S. Sarwar, D. Kirli, J. Shek, and A. Kiprakis, "A survey of second-life batteries based on techno-economic perspective and applications-based analysis," *Carbon Neutrality*, vol. 2, 04 2023.

[38] Y. Deng, Y. Zhang, F. Luo, and Y. Mu, "Hierarchical energy management for community microgrids with integration of second-life battery energy storage systems and photovoltaic solar energy," *IET Energy Systems Integration*, vol. 4, no. 2, pp. 206–219, 2022.

[39] Y. Deng, Y. Zhang, F. Luo, and Y. Mu, "Operational planning of centralized charging stations utilizing second-life battery energy storage systems," *IEEE Transactions on Sustainable Energy*, vol. 12, no. 1, pp. 387–399, 2021.

[40] W. Liu, T. Placke, and K. Chau, "Overview of batteries and battery management for electric vehicles," *Energy Reports*, vol. 8, pp. 4058–4084, 2022.

[41] A. Bera, S. Almasabi, Y. Tian, R. H. Byrne, B. Chalamala, T. A. Nguyen, and J. Mitra, "Maximising the investment returns of a grid-connected battery considering degradation cost," *IET Generation, Transmission & Distribution*, vol. 14, no. 21, pp. 4711–4718, 2020.

[42] H. Rallo, L. Canals Casals, D. De La Torre, R. Reinhardt, C. Marchante, and B. Amante, "Lithium-ion battery 2nd life used as a stationary energy storage system: Ageing and economic analysis in two real cases," *Journal of Cleaner Production*, vol. 272, p. 122584, 2020.

[43] A. Gad, "Particle swarm optimization algorithm and its applications: A systematic review," *Archives of Computational Methods in Engineering*, vol. 29, p. 2531–2561, 04 2022.

[44] V. Miranda, "EPSO AND DEEPSO: EVOLUTIONARY PARTICLE,"

[45] L. Xu, B. Song, and M. Cao, "An improved particle swarm optimization algorithm with adaptive weighted delay velocity," *Systems Science Control Engineering*, vol. 9, pp. 188–197, 02 2021.

[46] V. Miranda, H. Hrvoje, and Jaramillo Duque, "Stochastic star communication topology in evolutionary particle swarms (EPSO)," vol. 4, no. 2.

[47] Rstudio, "Evolutionary search," 2023.

[48] A. S. Pacheco and J. T. Saraiva, "An evolutionary particle swarm optimization, epso, approach to optimize the operation of hydro stations in market environment," in *11th International Conference on the European Energy Market (EEM14)*, pp. 1–6, 2014.

[49] V. Miranda, L. de Magalhaes Carvalho, M. A. da Rosa, A. M. L. da Silva, and C. Singh, "Improving power system reliability calculation efficiency with epso variants," *IEEE Transactions on Power Systems*, vol. 24, no. 4, pp. 1772–1779, 2009.

[50] E. H.-P. C. J. Undertaking, "Deucalion: a new eurohpc world-class green supercomputer in portugal," 2023.

[51] V. Delapedra-Silva, P. Ferreira, J. Cunha, and H. Kimura, "Methods for financial assessment of renewable energy projects: A review," *Processes*, vol. 10, no. 2, 2022.

[52] M. S. Cengiz, M. S. Mamis, M. Akdağ, and Çiğdem Cengiz, "A review of prices for photovoltaic systems," 2015.

[53] S. Quoilin, K. Kavvadias, A. Mercier, I. Pappone, and A. Zucker, "Quantifying self-consumption linked to solar home battery systems: Statistical analysis and economic assessment," *Applied Energy*, vol. 182, pp. 58–67, 2016.

[54] A. Komilov, "Location and orientation based lcoe: Simplified visual analysis and generalization of the levelized cost of electricity from storageless photovoltaic systems," *International Journal of Energy Research*, vol. 45, no. 4, pp. 5649–5658, 2021.

[55] A. Belderbos, E. Delarue, and W. D'haeseleer, "Calculating the levelized cost of electricity storage," 2016.

[56] A. Kirmas and R. Madlener, "Economic viability of second-life electric vehicle batteries for energy storage in private households," 2016.

[57] V. V. Viswanathan, A. J. Crawford, E. C. Thomsen, N. Shamim, G. Li, Q. Huang, and D. M. Reed, "An overview of the design and optimized operation of vanadium redox flow batteries for durations in the range of 4ndash;24 hours," *Batteries*, vol. 9, no. 4, 2023.